Broadband transponder based on coupled antenna elements and phased modulators

Prabhat Khanal

School of Electrical Engineering

Thesis submitted for examination for the degree of Master of Science in Technology.

Espoo 30.06.2018

Thesis supervisors:

Prof. Ville Viikari

Thesis advisor:

Univ. Lect. Jari Holopainen

Aalto University
School of Electrical
Engineering

AALTO UNIVERSITY
SCHOOL OF ELECTRICAL ENGINEERING

ABSTRACT OF THE
MASTER'S THESIS

Author: Prabhat Khanal

Title: Broadband transponder based on coupled antenna elements and phased modulators

Date: 30.06.2018 Language: English Number of pages: 8+41

Department of Electronics and Nanoengineering

Professorship: Radio Science and Engineering

Supervisor: Prof. Ville Viikari

Advisor: Univ. Lect. Jari Holopainen

A broadband transponder was studied over a frequency range of 1-6 GHz, which had strongly coupled antenna elements and phase variable modulators, and its performance was compared with a reference transponder which had a single antenna element connected to a single modulator. First, the transponders were mathematically modelled and their performances were studied through computer simulations. Then, the transponders were prototyped/demonstrated and their performances were studied through measurements.

In both simulations and measurements, it was found that the studied transponder with constantly phased modulators performed better than the reference transponder over a frequency range of 1-6 GHz. The studied transponder performed up to 40 dB higher at certain frequencies (e.g. at 1 GHz) compared with the reference transponder in both simulations as well as in measurements.

In addition to this, the performance of the studied transponder with optimally phased modulators was further increased up to 10 dB at certain frequencies in simulations. The received power of the studied transponder was measured only for five random samples of phase values. Even with these five randomly sampled phase values, it was found that the performance of the studied transponder with the sampled phased modulators increased up to 6 dB at certain frequencies, compared with the studied transponder with constantly phased modulators.

Keywords: transponder, broadband, wideband, ambient, backscatter, modulator, mixer, coupled antenna array, matching efficiency.

Preface

This thesis is the final part of my masters studies. It is based on the research work I did at the Department of Electronics and Nanoengineering, School of Electrical Engineering, Aalto University.

First and foremost, I would like to express my deepest gratitude to my supervisor Prof. Ville Viikari and my advisor Univ. Lect. Jari Hopolainen who have supported me throughout my thesis work with their patience, motivation and immense knowledge. I am highly obliged to be a part of their research group, which helped me in exploiting my potential. Their suggestions and feedbacks have supported me to achieve desired results in the most efficient ways. I am heartily thankful to them for the encouragement, supervision and support from the preliminary to the concluding level, which enabled me to develop a good understanding of the subject.

I would also like to thank Univ. Lect. Clemens Icheln for his valuable suggestions and comments during the measurements. I would also like to thank Dr. Kari Stadius and Dr. Enrico Roverato from integrated circuit design team, Department of Electronics and Nanoengineering, Aalto University for allowing me to use their logic analyser. Lastly, I would like to thank research engineer Matti Vaaja, who helped me to order the PCB and electronic components from the vendors.

Otaniemi, 30.06.2018

Prabhat Khanal

Contents

Symbols and abbreviations

Symbols

$[a]$	Incident voltage wave column vector $[V]$
a_i	Incident voltage wave at i^{th} Port $[V]$
$[b]$	Reflected voltage wave column vector $[V]$
b_i	Reflected voltage wave at i^{th} Port $[V]$
c	Speed of light $\approx 3 \times 10^8$ $[m/s]$
d	Time domain delay $[s]$
d_n	Time domain delay on n^{th} modulator $[s]$
$\lvert\delta\rho\rvert$	Change in the reflection coefficient between short and open circuit $= \lvert\rho_1 - \rho_2\rvert$
f	Frequency $[Hz]$
f_1, f_{RF}	Frequency of the transmitted signal $[Hz]$
f_m	First harmonic frequency of the switch control signal $[Hz]$
f_2, f_{osc}	Frequency of the signal produced by the oscillator $[Hz]$
G_r	Gain of the receiving antenna
G_t	Gain of the transmitting antenna
ϕ	Phase $[rad]$
P_r	Receive power $[W]$
P_t	Transmit power $[W]$
$RF1$	Output 1 of the switch in modulator PCB
$RF2$	Output 2 of the switch in modulator PCB
$RF - COM$	Input of the switch in modulator PCB
ρ	Reflection coefficient
ρ_1	Reflection coefficient when the load impedance at the output of the switch is zero ohms (i.e. short circuit)
ρ_2	Reflection coefficient when the load impedance at the output of the switch is infinite ohms (i.e. open circuit)
ρ_{in}	Input reflection coefficient
ρ_{in1}	Input reflection coefficient at Port 1
ρ_{load}	Frequency domain reflection coefficient when the load switches between short and open circuit
ρ_{loadn}	Frequency domain reflection coefficient when the load switches between short and open circuit at n^{th} Port
$\rho(t)$	Time domain reflection coefficient when the load switches between short and open circuit
$[S]$	Scattering matrix of the antenna model $[V]$
S_{ij}	Scattering parameter of i^{th} row and j^{th} column $[V]$
t	Time $[s]$
T	Period of the switch control signal $[s]$
ω	Angular frequency $[rad/s]$
ω_1, ω_{RF}	Angular frequency of the transmitted signal $[rad/s]$
ω_m	Angular frequency of the first harmonic in the switch control signal $[rad/s]$
ω_2, ω_{osc}	Angular frequency of the oscillator signal $[rad/s]$
Z_0	Characteristic impedance of 50 ohms transmission line $[\Omega]$
Z_L	Load impedance $[\Omega]$

Abbreviations

AC	Alternating current
APLAC	An object-oriented analogue circuit simulator and design tool (originally Analysis Program for Linear Active Circuits)
CPU	Central processing unit
CST	Computer simulation technology, electromagnetic simulation software
DC	Direct current
EM	Electromagnetic
GPS	Global positioning system
HB	Harmonic balance
IoT	Internet of thing
MIMO	Multiple in, multiple out
NI AWR	National instruments applied wave research, circuit simulation and design software
PCB	Printed circuit board
RBW	Resolution bandwidth
RF	Radio frequency
RFID	Radio frequency identification
RFMEMS	Radio frequency micro-electromechanical system
Rx	Receiver
SMA	SubMiniature version A, a type of coaxial RF connectors
SMD	Surface mount device
SPDT	Single pole, dual throw
Tx	Transmitter
UHF	Ultra high frequency
VBW	Video bandwidth
VNA	Vector network analyser
Wi-Fi	Trademark for WLANs
WLAN	Wireless Local Area Network
WSN	Wireless sensor network

List of Figures

1 Introduction

A radio frequency (RF) transponder is a device, which receives a radio signal and automatically transmits a different signal [1]. This different signal is received by another radio device, which would process and extract the information contained in the signal. RF transponders are used for many different applications. Traditionally, they were used in auto-identification systems, like radio frequency identification (RFID) [2] and sensing/monitoring systems like wireless sensors and actuators [3]. However, due to advances in digital electronics and computing, more recently the transponders are also being used in internet of things (IoTs) [4] and distributed computing systems [5].

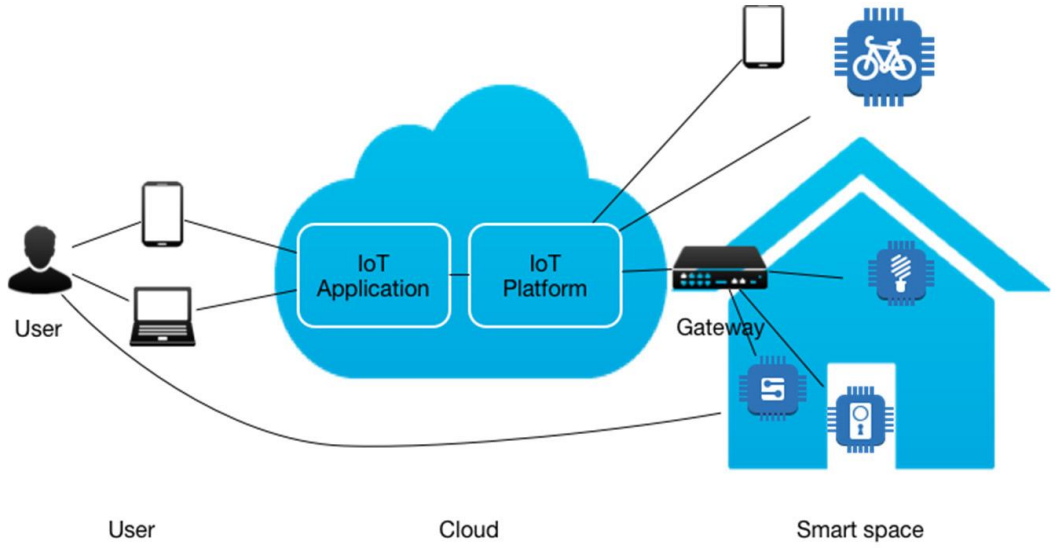

Fig. 1. Basic internet of things (IoT) architecture [4].

The transponders are traditionally connected through a direct radio link to a base station, which is locally connected to a central processing unit (CPU). However, as shown in Fig. 1 IoT platform connects these transponders to the CPU over the internet cloud. Depending upon the deployment of the IoT systems, these wireless sensors can process the information data and communicate with each other independent of the CPU. Some of the computation is done in the wireless sensors while the CPU is used only for certain computational tasks. This kind of computing system is called distributed computing system.

Recently, ambient backscatter communications have been introduced as a cutting-edge technology which enables smart devices to communicate by utilizing ambient RF signals without requiring an active RF transmission [6]. This technology is especially effective in addressing communication and energy efficiency problems for low-power communication systems, such as sensor networks. The ambient backscattering principle is a very promising way to realize batteryless wireless connections in future

IoTs. However, to fully exploit available ambient energy, the antenna needs to tune its operation to a frequency where the highest ambient power is available.

Mainly, four techniques are being applied in the execution of frequency reconfigurable antennas [7]. Firstly, Electrical reconfiguration which can be implemented with Radio Frequency-Micro Electro Mechanical System switches (RF MEMS), PIN diodes, and varactor diodes. Secondly, Optical reconfigurable antennas are those which use photoconductive switching elements such as silicon switches for frequency reconfiguration. Thirdly, physical reconfigurable antennas which are based on the reconfiguration obtained by the structural alteration of the antenna using slots, cuts, etc. Finally, smart materials like liquid crystals, ferrites etc. are also being used for the reconfiguration of antennas. All of these techniques are analogue techniques, and they change the electrical or physical length of the antennas.

This thesis is however inspired by the frequency reconfigurable concept presented in [8]. Unlike the techniques in [7], in [8] frequency reconfiguration is done by using properly weighted incident signals to the antenna inputs. The weighting of these inputs can be done in the digital part of the transceiver. The biggest benefit of this technique is that the antenna structure works over a relatively large frequency range. Also, the digital electronics develop fast therefore digital methods develop faster than analogue methods.

There are no RF transponders which utilize the concept presented in [8] that are known to the author. Therefore, the novelty of this thesis is to study the concept of frequency reconfigurable RF transponder using the techniques presented in [8]. An almost similar method based on a number of antenna elements might be used to redirect the re-scattered signal to any direction. In the future, a transponder with a number of antenna elements might be used for "transponder MIMO" operation. Carrier aggregation might be possible as well.

Whereas, this thesis only studies the feasibility of such a frequency reconfigurable transponder. A broadband transponder with strongly coupled antenna elements and phase variable modulators is studied over a frequency range of 1-6 GHz, and its performance is compared with a reference transponder with a single antenna element and a single modulator. At first, the transponders are mathematically modelled and their performances are studied through computer simulations. Then the transponders are prototyped/demonstrated and their performances are studied through measurements. Chapter 2 briefly discusses some background theories and concepts which are used in Chapter 3 to model the transponders mathematically. Chapter 3 also contains the results and its analyses obtained during the computer simulations. In Chapter 4, the transponders are prototyped/demonstrated, and measurements are performed. It also contains the measurement results and its analyses. Finally, Chapter 5 briefly concludes the thesis work. It discusses the findings and observations of the thesis work and gives some suggestions for further studies.

2 General background

This chapter gives a general background of transponders. Section 2.1 briefly discusses wireless sensor networks, their uses and how they are related to the work of this thesis. Next, Section 2.2, briefly discusses a traditional model of an RF transponder. After that, Section 2.3 presents a concept antenna from an article, which inspired the transponder model used in this thesis. Sections 2.4, 2.5 and 2.6 discuss some general theories and concepts, which are used in Chapter 3 to model the transponder studied in the thesis mathematically.

2.1 Wireless sensor network

A sensor is a device which detects or measures physical property and records, indicates, or otherwise responds to it. An electronic sensor senses its surroundings by converting the environmental stimulus into an electronic signal [9]. For example, an accelerometer measures the acceleration of an object, magnetometer measures the magnetic field strength, gyroscope measures the rotation velocity, barometer measures the atmospheric pressure, hygrometer measures the relative humidity in the environment, and so on [10].

Traditionally, these sensors were wired devices connected to a central processing unit (CPU). When more than one sensors are connected to the CPU by a wired connection, it becomes a wired sensor network, and each sensor device becomes a sensor node. This kind of network is good for a small number of sensor nodes in indoor environments. However, when the number of sensor nodes becomes large, it becomes very difficult to manage the cables running to the CPU, and increases the cabling costs and installation time. Additionally, a wired sensor network needs to have new physical connections to the CPU hardware whenever new nodes are added to the network. Because of these difficulties, nowadays wireless sensor networks (WSN) is gaining more attraction. In WSN, the nodes are wirelessly connected to the CPU. It is an emerging technology that promises a wide range of potential applications, therefore, it has been an active field of research and engineering in both academia and industry in recent years [11].

A WSN consists of an array of inexpensive small sensor nodes with sensing, data processing, and communication capabilities. These nodes are densely deployed in a region of interest and they collaborate to accomplish a common task and forward the data to a base station located on the periphery of the sensor network. The base station collects the data from the sensor nodes and transmits this data to a physical CPU via a wired connection or through the internet for computation [12]. Sensor nodes can be either thrown in as a mass or placed one by one in the sensor field, and its position need not be engineered or predetermined. This allows the deployment of the sensor nodes in inaccessible terrains such as disaster relief operations [13] and in gas turbine engines [14]. Dramatic advances in wireless communication and electronics have reduced the cost of the sensor nodes, which in turn enable the use

of a large scale low cost, low powered multifunctional sensor nodes that are small in size and communicate at short distances [15].

Combined with the technologies like the global positioning system (GPS), cloud computing and internet of things (IoT); WSNs can be deployed in a global, scale such that, they sense/monitor and record the data of various locations [16]. A new generation of multi-protocol Bluetooth/802.15.4/WiFi chips have accelerated the growth of WSNs as the network incompatibility argument fades away and IoT applications become the primary differentiator. By 2023, there will be 3.4 billion annual WSN chipset shipments worldwide, up from 1 billion in 2018 [17].

Each sensor node is equipped with a sensing unit, a low computational capacity processor, a short-range wireless transmitter-receiver and an optional limited battery supplied energy. This thesis aims to study the transmitter-receiver unit of a node. For this thesis, the base station would be the reader device and the sensor node would be a single transponder.

2.2 Traditional transponder model

An RF transponder, which is used in WSNs, generally operates at microwave frequencies [3]. Microwaves are electromagnetic waves of frequency 300 MHz to 300 GHz. Common transponders used in microwave frequencies are ultra high frequency (UHF) radio frequency identification (RFIDs), Bluetooth and Zig-bee transponders.

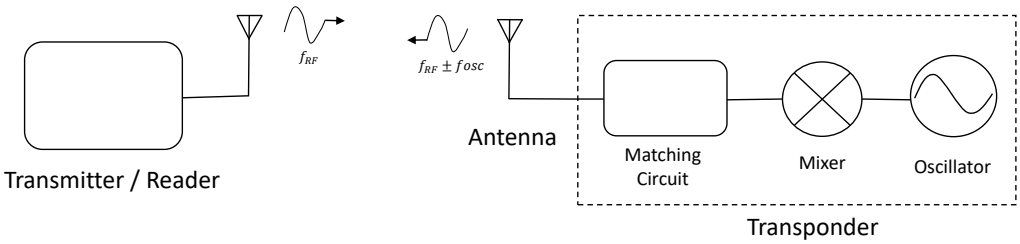

Fig. 2. Block diagram of a simple traditional transponder model.

A simple traditional transponder model used in UHF RFIDs is shown in Fig. 2. This model consists of the antenna, matching circuit, mixer and oscillator. These components are explained briefly as follow:

1. **Antenna:**
   An antenna is an electrical component, which converts radio waves into an electrical current or vice versa. It is used to receive and transmit the radio waves [18]. It is usually made of a metallic conductor. Some of the important characteristics of an antenna are; its gain, directivity, radiation pattern, radiation

efficiency and the operational bandwidth. An antenna is a reciprocal device, meaning its characteristics are the same in both transmitting and receiving cases.

2. **Propagation channel:**
   A propagation channel is a space between transmitting and receiving antennas where radio waves propagate [19]. A receiving antenna receives less power than the power transmitted through a transmitting antenna due to the path loss in propagation channel. Power received by receiving antenna during free space propagation is given by Eq. (1).

$$P_r = P_t - 20\log_{10}(d) - 20\log_{10}(f) - 20\log_{10}(4\pi/c) + G_t + G_r. \quad (1)$$

   where P_r is received power, P_t is transmitted power, d is the distance between transmitting and receiving antennas, f is operating frequency, G_t is gain of transmitting antenna, G_r is gain of receiving antenna and c is the speed of light.

3. **Matching circuit:**
   A matching circuit changes the input impedance of an electrical load to minimize the voltage or power reflections to the circuit or changes the output impedance of its corresponding signal source to maximize the power transfer to the rest of the circuit [20, p 228-266]. The matching circuit can be built by lumped components like inductors and capacitors. In high frequencies, the matching circuit can be built using microstrip lines like half wave or quarter wave transformers. A matching circuit is a resonant based circuit, therefore it operates at the resonance frequency and has a limited bandwidth. Adding more resonator would increase the bandwidth of a matching circuit but it would still be limited due to bode fano criteria [20, p. 266],[21].

4. **Mixer:**
   A mixer is a non-linear electrical component, which inputs two or more signals of different frequencies and outputs a signal whose frequency components are sum and difference of the input signal frequencies [20, p. 637]. The mixer is discussed more in Section 2.4.

5. **Oscillator:**
   An oscillator is an electrical component, which outputs a defined signal [20, p. 604]. In simple transponders, this could be a sinusoidal oscillator at a single frequency. However, in more complex transponders, for example; in a wireless sensor node, this would be the sensing and computing unit. The sensing unit would sense the environment and send an electronic signal to the computing unit. After the computation, it produces an output signal containing the sensed data which is required to transmit to the base station/reader. In this case,

the sensing and computing unit of the sensor node are collectively modelled as an electronic oscillator. The output frequency of the oscillator contains the information of the transponder.

Apart from these, the transponder model can also have filters to filter out unwanted signals, a battery to power on the active transponder, rectifier network to harvest the RF signal and power the transponder, indicators to indicate the user about something, and so on [2]. The reader is a radio device, which has a transmitter-receiver circuit. It transmits an RF signal to the transponder and receives the RF signal which is transmitted by the transponder. The reader is connected to the central processing unit which decodes the information signal sent by the transponder and uses the information for its intended application.

In Fig. 17, the reader sends an RF signal of frequency f_{RF} to the transponder. The transponder antenna receives the RF signal. The received signal passes through the matching network and reaches the mixer. The oscillator produces a signal of frequency f_{osc}. The received signal and the oscillator signal inputs the mixer, and it outputs the signal of frequency $f_{RF\pm osc}$. This signal returns to the transponder antenna through the matching circuit. The transponder antenna radiates and transmits the signal of frequency $f_{RF\pm osc}$ to the reader. The reader receives this signal and gets the information signal f_{osc} of the transponder.

However, the transponder model used in this thesis is different from the traditional model studied in this section. The transponder model used in the thesis has an array of modulators connected to a strongly coupled antenna elements cluster.

2.3 Coupled antenna Cluster

Feasibility of a broadband transponder is studied in this thesis. As discussed briefly in Section 2.2, usually, the impedance matching limits the operational bandwidth in traditional transponders. Therefore, in this thesis, a new transponder concept is studied which does not need a matching circuit.

Jari-Matti Hannula et. al. present a concept of a frequency reconfigurable antenna which can have broadband impedance matching without using a conventional matching circuit in [8]. Fig. 3 is a basic diagram of the antenna structure purposed in [8]. The antenna consists of multiple radiating elements that have strong mutual coupling between them. By properly weighting the incident signals a_i in each element, the reflected voltage wave b_i can be minimized and matching efficiency can be maximized. This kind of antenna structure is good for active radio devices because, in this technique, the incident signal in each antenna element a_i needs to be a variable phase and amplitude signal to reconfigure the antenna matching at different frequencies.

The power consumption of the variable gain amplifiers is high therefore, they are hard to implement in a passive or battery assisted transponders. Because of this

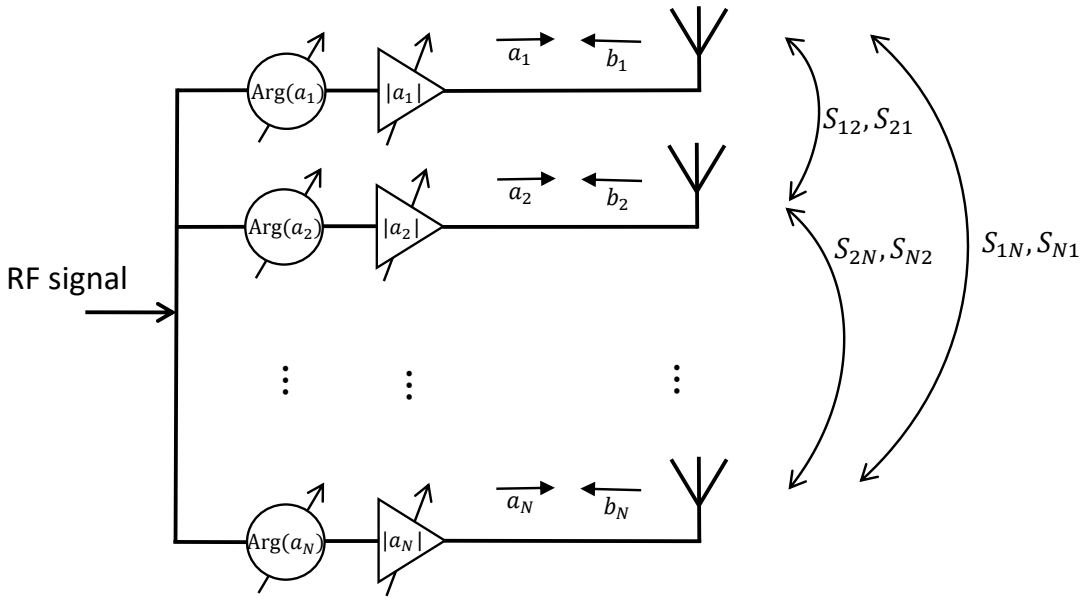

Fig. 3. Coupled antenna concept presented in [8].

reason, the transponder studied in this thesis does not have any gain amplifiers at the inputs of antenna elements. Similar to antenna structure presented in [8], the antenna used for the transponder in this thesis also consists of multiple elements that have strong mutual coupling between them. However, unlike in [8], the incident signals of each antenna elements are constant amplitude and variable phase signals. This will not give the matching efficiency as high as the antenna of [8]. However, this might give better matching efficiency compared with a constant phase and constant amplitude transponder.

This thesis aims to study the received power of a transponder whose inputs of the antenna elements have the constant phase and amplitude signals compared with that of the variable phase and constant amplitude signals. The antenna structure used in this thesis is discussed more in Chapter 3.

2.4 Switch as a Mixer

A mixer is a device which combines two or more electronic signals of different frequencies and produces an output signal, whose frequencies are sum and difference of the input signals [20, p. 637]. It either uses non-linear properties of a diode or transistor or uses a time varying element of the circuit, to achieve the frequency conversion. The mixer is one of the key components which is used in Chapter 3 to model the transponder.

Fig. 4 is a block diagram of a simple and ideal 3 port mixer, which inputs signals of frequency f_1 and f_2 through Port 1 and 2 respectively, and outputs a signal of frequency $f_1 + f_2$ and $f_1 - f_2$ through Port 3 [20, p. 637]. In an ideal mixer, when

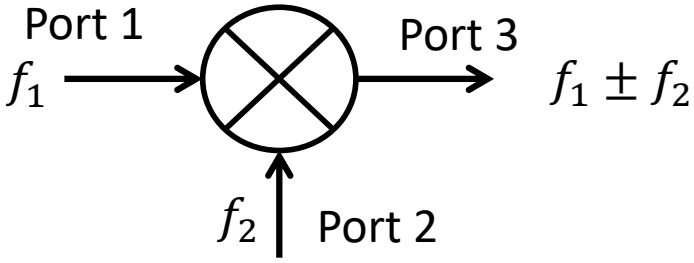

Fig. 4. An ideal 3 port mixer where Port 1 and Port 2 are inputs and Port 3 is output.

the input signal at Port 1 is $cos(\omega_1 t)$ and Port 2 is $cos(\omega_2 t)$, the output signal at Port 3 would be a product of these two input signals as Eq. (2).

$$cos(\omega_1 t)cos(\omega_2 t) = Kcos((\omega_1 + \omega_2)t) + cos((\omega_1 - \omega_2)t) \ , \tag{2}$$

where K is constant which accounts for the voltage conversion loss in the mixer.

Usually, at RF and microwave frequencies, mixers are made by exploiting non-linear properties of non-linear electronic components, like; diodes and transistors. However, in this project, the mixer is made by using a time-varying element. Fig. 5 shows the block diagram of the mixer used in this project. Here, the input signal of a switch is switched between two loads, short circuit (zero impedance) and open circuit (infinite impedance) using a switch control signal. The switch control signal is a periodic square wave signal of period $1/f_m$.

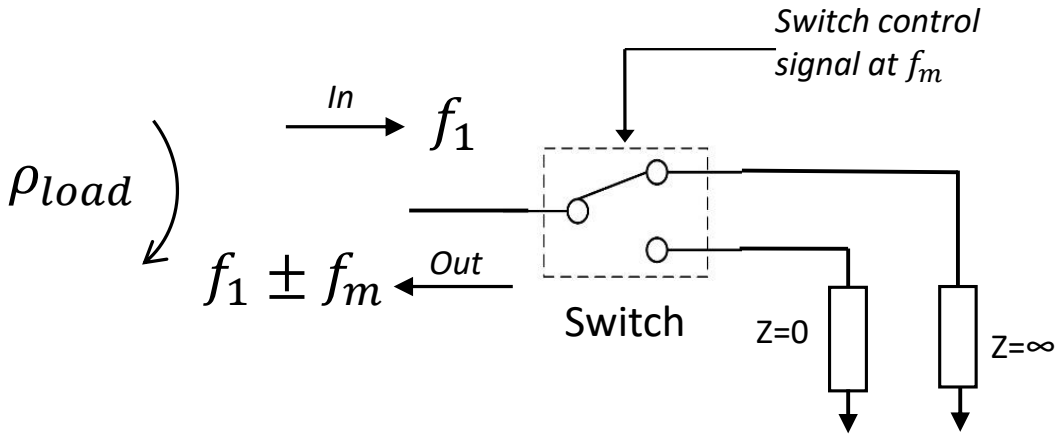

Fig. 5. An ideal switch switching between zero and infinite ohms load impedance where $f_m << f_1$.

The Fourier series of a square wave gives an odd number of harmonics, as shown in Fig. 6. This means a square wave of period $1/f_m$ has sinusoidal signals of frequencies f_m , $3f_m$, $5f_m$, and so on [22]. When a signal of frequency f_1 (where $f_1 >> f_m$) inputs the switch, it will get mixed with the harmonics of the square wave as in Eq. (2), and becomes a mixed signal of frequencies $f_1 \pm f_m$, $f_1 \pm 3f_m$, $f_1 \pm 5f_m$, and so on. Since the load is switching between a short and open circuit (creating reflection coefficients -1 and +1 respectively), the mixed signal would reflect back at the input of the switch. Hence, the time-varying switch produces the mixed signal and works like a mixer. The switching of load impedances creates a modulation, therefore this circuit is also called a modulator.

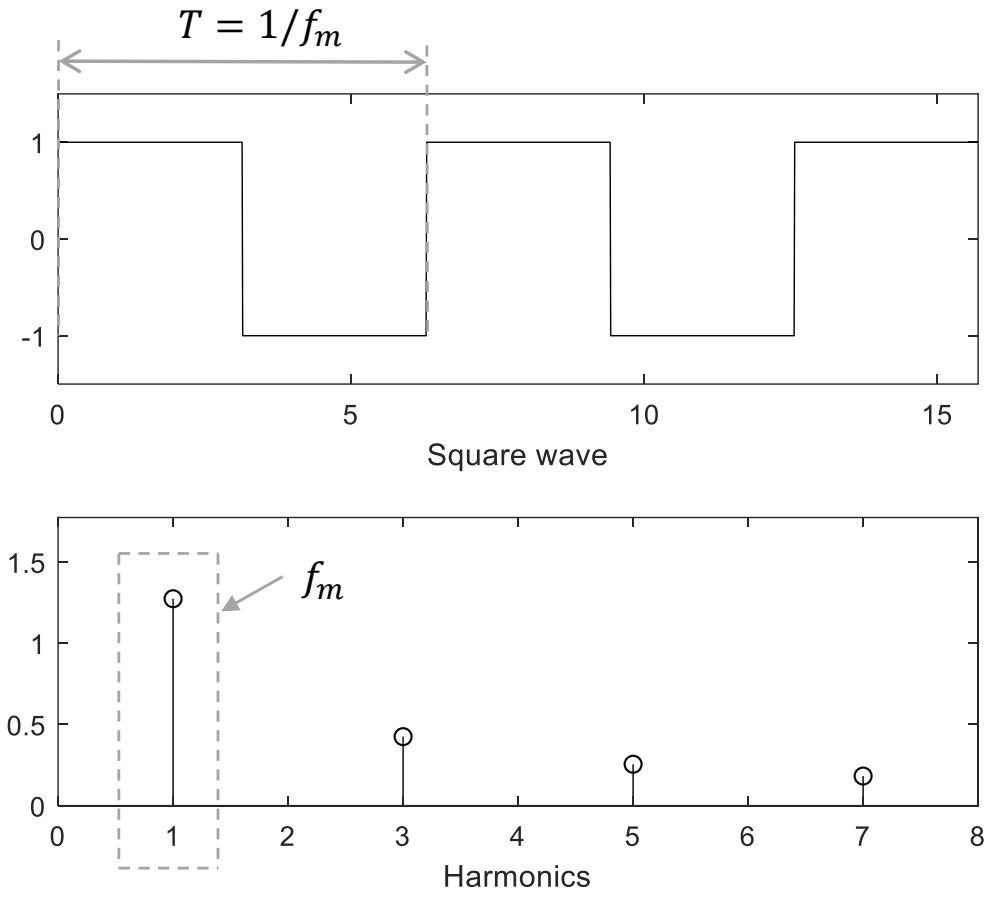

Fig. 6. A square wave and its Fourier series harmonics.

The port impedance of the switch is 50 ohms. When the load is switched between zero and infinite ohms, it creates a time domain reflection coefficient ($\rho(t)$) at the input of the switch, which varies between $\rho_1 = -1$ and $\rho_2 = +1$ respectively. The modulated reflection coefficient at the input of the switch due to the modulating loads in the frequency domain ρ_{load}, would be the Fourier series of the time domain reflection coefficient ρ over one period. This is calculated as:

$$\rho_{load}(\omega_m) = \frac{1}{T}\int_0^T \rho(t)\ e^{-j\omega_m t}dt$$

$$= \frac{\omega_m}{2\pi}\left(\int_d^{d+\pi/\omega_m} \rho_1\ e^{-j\omega_m t}dt + \int_{d+\pi/\omega_m}^{d+2\pi/\omega_m} \rho_2\ e^{-j\omega_m t}dt\right).$$

This becomes

$$\rho_{load} = \frac{-j}{2\pi}\ e^{-2jd\omega_m}(e^{jd\omega_m}(2\rho_1 - \rho_2) - \rho_2), \tag{3}$$

and when $d = 0$,

$$\rho_{load} = \frac{-j}{\pi}(\rho_1 - \rho_2)\ , \tag{4}$$

where, T is one period of the square wave, and d is a time instance from where one period of square wave starts.

Eq. (3) gives the modulated reflection coefficient ρ_{load} at the first harmonic. The performances of the transponders studied in this thesis are studied at the first harmonic only, therefore Eq. (3) is enough to model the studied transponders. It is good to note that in Eq. (4), the amplitude of ρ_{load} is directly proportional to the difference between ρ_1 and ρ_2, and is independent of ω_m when $d = 0$.

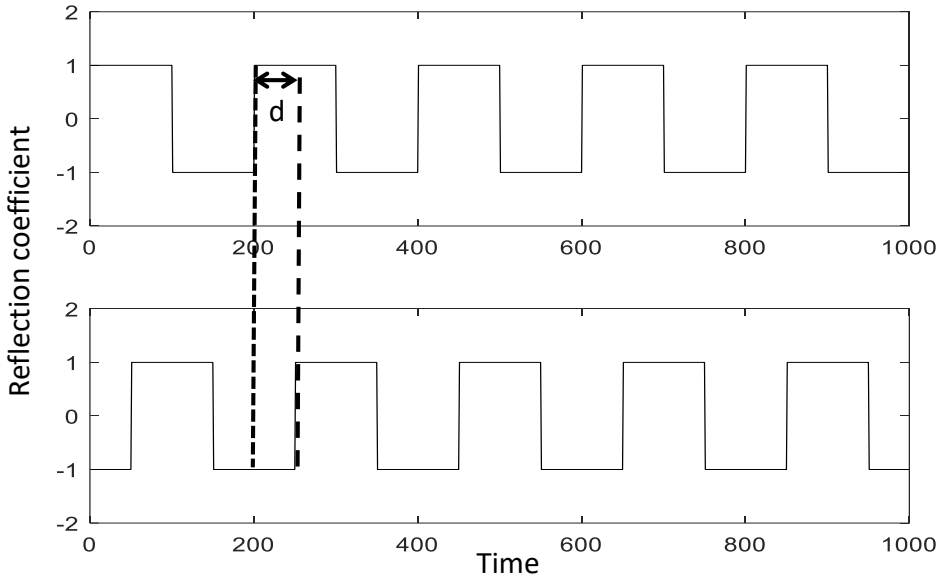

Fig. 7. Two switch control signals, one is delayed in time domain by d to create phase difference in phasor domain.

Later in this thesis, the transponder is modelled using multiple modulators. The outputs of the modulators are connected to a multi-element coupled antenna. As discussed in Section 2.3, each of these elements inputs a constant amplitude and variable phase signals. To create the phase difference between the outputs of the modulators, the switch control signals of these modulators are delayed in the time domain as shown in Fig. 7. This is done because a delay in the time domain creates a phase difference in the phasor domain as shown in Eq. (5). The switch control signal of the first modulator is taken as a reference signal and the rest of the modulators are delayed compared to this reference signal as shown in Fig. 7.

$$cos(\omega t) \xrightarrow{delayed} cos(\omega(t-d)) = cos(\omega t - \omega d) = cos(\omega t + \phi) \ , \tag{5}$$

where phase $\phi = -\omega d$.

In Eq. (3) d is a time instance where one period of square wave starts. This is the delay value discussed in Eq. (5) and it will create the phase difference of $-\omega_m d$ compared to when delay value is zero (i.e. $d = 0$).

2.5 Scattering parameters

A key assumption during measurements is that the electrical networks can be completely characterized by the quantities measured at the network terminals (ports) regardless of the contains of the networks [23]. Generally, at low frequencies, Z-parameters and Y-parameters are used to characterize the network. However, at microwave frequencies, scattering parameters are preferred. This is because at high frequencies they are easier to measure and work with it than other kinds of parameters. They are conceptually simple, analytically convenient, and capable of providing a great insight into a measured or design problem.

Let us consider an N-port microwave network as shown in Fig. 8, where the voltage waves incident to the ports are $a_1, a_2, a_3, ..., a_N$, and voltage waves reflected from the ports are $b_1, b_2, b_3, ..., b_N$. Then, the scattering matrix **S** is defined as:

$$\begin{bmatrix} b_1 \\ b_2 \\ \dots \\ b_N \end{bmatrix} = \begin{bmatrix} S_{11} & S_{12} & \dots & S_{1N} \\ S_{21} & S_{22} & \dots & S_{2N} \\ \vdots & \vdots & \ddots & \vdots \\ S_{N1} & S_{N2} & \dots & S_{NN} \end{bmatrix} \begin{bmatrix} a_1 \\ a_2 \\ \dots \\ a_N \end{bmatrix}$$

or,

$$[\mathbf{b}] = [\mathbf{S}][\mathbf{a}], \tag{6}$$

where **b** is the reflected wave column vector and **a** is the incident wave column vector. Elements of the scattering matrix are called scattering parameters or S-parameters.

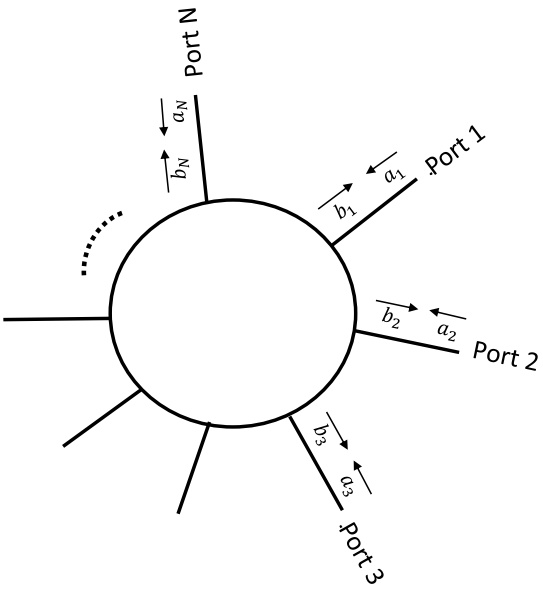

Fig. 8. An N port microwave network.

The specific S-parameters are defined as:

$$S_{ij} = \frac{b_i}{a_j}, \text{ when } a_k = 0 \text{ for } k \neq j. \tag{7}$$

Eq. (7) shows that S_{ij} is found by exciting the port j by a voltage wave a_j and measuring the reflected voltage wave b_i coming out of port j when the other ports are perfectly matched. In other words, when ports other than j are terminated with the load impedance of respective ports.

2.6 Input reflection coefficient of an N-port system

The voltage reflection coefficient is defined as a ratio of the reflected voltage wave to the incident voltage wave, at an electrical terminal or port [20, p. 57]. The voltage reflection coefficient of the load impedance Z_L with respect to a characteristic impedance Z_0 at a port as shown in Fig. 9 is given by Eq. (8).

$$\rho = \frac{\text{Reflected voltage wave}}{\text{Incident voltage wave}} = \frac{Z_L - Z_0}{Z_L + Z_0}. \tag{8}$$

The voltage wave incident to a matched port (i.e. $Z_L = Z_0$) does not have any reflected voltage waves. All the incident waves are absorbed by the load. However, if the port is not properly matched (i.e. $Z_L \neq Z_0$), the load will reflect some of the voltage waves at that port. If an N-port microwave network does not have perfectly isolated ports, the reflected voltage waves at a port would travel to other port. These reflected voltage waves seen at other port are dependent upon the scattering

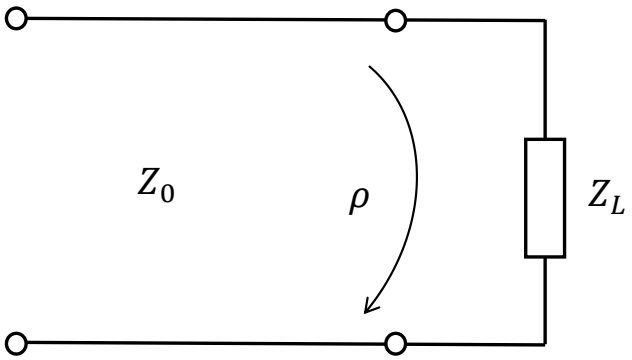

Fig. 9. A port of characteristic impedance Z_0 terminated with a load impedance Z_L.

parameters and the load impedances at the ports of the network. Therefore, a multi-port model is needed to study an N-port network and their load impedances. In addition to this, a multi-port model also includes mutual coupling between its ports, which a single port model does not. The multi-port model is very useful in this thesis where the transponder antenna has strongly coupled multiple elements antenna.

In this section, the input reflection coefficient of an N-port microwave network is studied. The following derivation is applied from [24]. Let us consider an N-port network of the scattering matrix **S** as shown in Fig. 10. The voltage waves incident to the Ports $1, 2, 3, ..., N$ are $a_1, a_2, a_3, ..., a_N$, and the voltage waves reflected from the Ports $1, 2, 3, ..., N$ are $b_1, b_2, b_3, ..., b_N$.

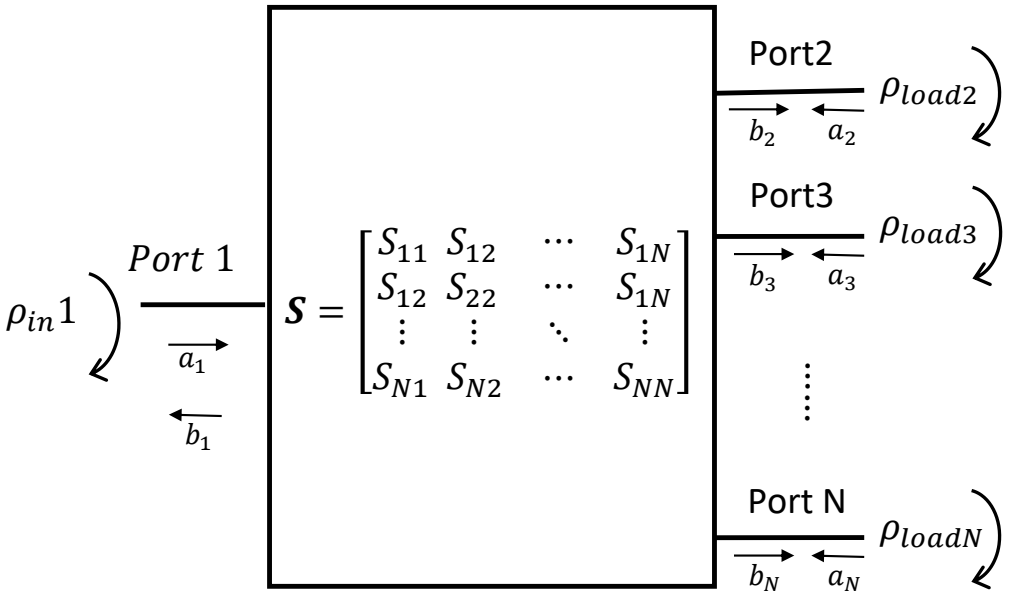

Fig. 10. An N-port microwave network.

The input reflection coefficient at Port 1 is:

$$\rho_{in1} = \frac{b_1}{a_1}, \tag{9}$$

and the load reflection coefficients at Ports $2, 3, ..., N$ are:

$$\rho_{loadn} = \frac{a_n}{b_n} \text{ where, n= 2,3,...,N.} \tag{10}$$

From the definition of the scattering matrix in Section 2.5, Eq. (6) can be written as:

$$[\mathbf{b}] = \begin{bmatrix} b_1 \\ b_2 \\ \dots \\ b_N \end{bmatrix} = [\mathbf{S}][\mathbf{a}] = \begin{bmatrix} S_{11} & S_{12} & \dots & S_{1N} \\ S_{21} & S_{22} & \dots & S_{2N} \\ \vdots & \vdots & \ddots & \vdots \\ S_{N1} & S_{N2} & \dots & S_{NN} \end{bmatrix} \begin{bmatrix} a_1 \\ a_2 \\ \dots \\ a_N \end{bmatrix} \tag{11}$$

Using Eq. (9) and (10), Eq. (11) can be rewritten as:

$$[\mathbf{b}] = \begin{bmatrix} b_1 \\ b_2 \\ \dots \\ b_N \end{bmatrix} = [\mathbf{S}][\mathbf{a}] = \begin{bmatrix} S_{11} & S_{12} & \dots & S_{1N} \\ S_{21} & S_{22} & \dots & S_{2N} \\ \vdots & \vdots & \ddots & \vdots \\ S_{N1} & S_{N2} & \dots & S_{NN} \end{bmatrix} \begin{bmatrix} b_1/\rho_{in1} \\ b_2\rho_{load2} \\ \dots \\ b_N\rho_{loadN} \end{bmatrix}$$

$$= \begin{bmatrix} S_{11} & S_{12} & \dots & S_{1N} \\ S_{21} & S_{22} & \dots & S_{2N} \\ \vdots & \vdots & \ddots & \vdots \\ S_{N1} & S_{N2} & \dots & S_{NN} \end{bmatrix} \begin{bmatrix} 1/\rho_{in1} & 0 & \dots & 0 \\ 0 & \rho_{load2} & \dots & 0 \\ \vdots & \vdots & \ddots & \vdots \\ 0 & 0 & \dots & \rho_{loadN} \end{bmatrix} \begin{bmatrix} b_1 \\ b_2 \\ \dots \\ b_N \end{bmatrix}$$

or,

$$[\mathbf{b}] = \begin{bmatrix} S_{11}/\rho_{in1} & S_{12}\rho_{load2} & \dots & S_{1N}\rho_{loadN} \\ S_{21}/\rho_{in1} & S_{22}\rho_{load2} & \dots & S_{2N}\rho_{loadN} \\ \vdots & \vdots & \ddots & \vdots \\ S_{N1}/\rho_{in1} & S_{N2}\rho_{load2} & \dots & S_{NN}\rho_{loadN} \end{bmatrix} \begin{bmatrix} b_1 \\ b_2 \\ \dots \\ b_N \end{bmatrix} = [\mathbf{A}][\mathbf{b}]$$

or,

$$\mathbf{(A\text{-}I)b} = 0, \tag{12}$$

where $\mathbf{I}$ is an identity matrix. The matrix $\mathbf{A}$ contains the unknown variable: ρ_{in1} and known variables: s-parameters and ρ_{loadn}.

The Eq. (12) has two solutions. The first solution is when $\mathbf{b}$ equals a zero column vector. In this case, the reflected voltage waves $b_1, b_2, ..., b_N$, all equals to

zero. Using Eq. (9) and (10), the input reflection coefficient ρ_{in1} and the reflection coefficients at loads $\rho_{load2}, \rho_{load3}, ..., \rho_{loadN}$, all equals to zero as well. This means the input port is matched with the impedance of the source, and all other ports are matched with the load impedances. Port 1 is isolated from other ports, and there are no waves coming out of other ports. All the incident waves are consumed by the N-port network. Here, the aim is to find the input reflection coefficient of an N-port network, and input reflection coefficient equals to zero is not the desired solution.

When Port 1 is neither perfectly matched nor isolated, then $\mathbf{b} \neq 0$. In this case, for a solution of Eq. (12) to exist, the determinant of **(A-I)** is required to be zero.

$$\mathbf{det(A\text{-}I)} = \begin{vmatrix} S_{11}/\rho_{in1} - 1 & S_{12}\rho_{load2} & \dots & S_{1N}\rho_{loadN} \\ S_{21}/\rho_{in1} & S_{22}\rho_{load2} - 1 & \dots & S_{2N}\rho_{loadN} \\ \vdots & \vdots & \ddots & \vdots \\ S_{N1}/\rho_{in1} & S_{N2}\rho_{load2} & \dots & S_{NN}\rho_{loadN} - 1 \end{vmatrix} = 0$$

Using the square matrix properties, the determinant of a square matrix is equal to the determinant of its conjugate transpose [22].

$$\mathbf{det(A\text{-}I)} = \mathbf{det(A\text{-}I)'} = 0$$

or,

$$\begin{vmatrix} S_{11}/\rho_{in1} - 1 & S_{21}/\rho_{in1} & \dots & S_{N1}/\rho_{in1} \\ S_{12}\rho_{load2} & S_{22}\rho_{load2} - 1 & \dots & S_{N2}\rho_{load2} \\ \vdots & \vdots & \ddots & \vdots \\ S_{1N}\rho_{loadN} & S_{2N}\rho_{loadN} & \dots & S_{NN}\rho_{loadN} - 1 \end{vmatrix} = 0 \tag{13}$$

Solving Eq. (13) gives,

$$\begin{aligned} \rho_{in1} &= \frac{S_{11}D_1 - S_{21}D_2 + S_{31}D_3 - ..... + S_{NN}D_N}{D_1}, \text{ for an odd number of N} \\ \rho_{in1} &= \frac{S_{11}D_1 - S_{21}D_2 + S_{31}D_3 - ..... - S_{NN}D_N}{D_1}, \text{ for an even number of N} \end{aligned} \tag{14}$$

where D_1 is the determinant of a matrix, which is created by removing the first row and the first column from the matrix **(A-I)'**, D_2 is the determinant of a matrix which, is created by removing the first row and the second column from the matrix **(A-I)'**, D_3 is the determinant of a matrix which, is created by removing the first row and the third column from the matrix **(A-I)'**, and so on.

When the scattering matrix **S** and the load reflection coefficients ρ_{loadn} are known, the input reflection coefficient ρ_{in1} can be solved from Eq. 14.

3 Simulated transponder model and results

The transponder studied in this thesis is different from the traditional transponder model discussed in Section 2.2. In this thesis, two transponder models are studied: 1) Broadband transponder based on four phased modulators and 2) Narrowband transponder based on a single modulator. The narrowband transponder is used as a reference, and its performance is compared with the broadband transponder. These two transponders are modelled using the theories studied in Sections 2.4, 2.5 and 2.6.

The purpose of this work is to study the feasibility of a broadband transponder based on a number of coupled antenna elements and phased modulators. Here the received power of a transponder based on four phased modulators is compared with the transponder based on four constant phase modulators, and with the transponder based on a single modulator. From here onwards, the transponder based on four modulators is designated as a studied transponder and the transponder based on a single modulator is designated as a reference transponder.

In this chapter, the reader and transponder antennas, and the propagation channel of the studied and reference transponders are introduced and modelled using CST Microwave Studio [25]. Then the scattering matrices of the CST models are extracted and mathematical models for the transponders are developed. These models are then simulated using MathWorks Matlab [26], and the received powers of the transponders are studied. The transponders are also simulated using AWR circuit simulator [27], and their received powers are studied. Finally, the results of these simulations are analysed.

3.1 Antenna and propagation channel model

The antenna model used for the studied transponder is shown in Fig. 11. It consists of four monopole antenna elements which, are grouped together in a 2×2 array, such that, they are spaced 25 mm diagonally. The lengths of the monopoles are 65 mm, 45 mm, 30 mm and 10 mm. These were selected such that their operational bands cover the frequency range from 1 to 6 GHz as shown in Fig. 13. The antenna model used for the reference transponder is shown in Fig. 12. It contains a single element monopole antenna, which is tuned at 3 GHz as shown in Fig. 14.

The reader antenna is the same for both antenna models. It is a finite biconical antenna [28]. Each cone of the biconical antenna has the vertex angle of 110 degrees and height of 85 mm. The biconical antenna has a very large bandwidth and it can illuminate the transponder antennas in the desired frequency range (1-6 GHz). The realized gain of the reader antenna is shown in Fig. 15. In both antenna models, the distance between the transponder and reader antenna is 0.85 m, and the thickness of the monopole antenna elements are 2 mm. Both of these antenna models were modelled in CST Microwave Studio, and their scattering matrices are exported (from CST) to model the transponder mathematically.

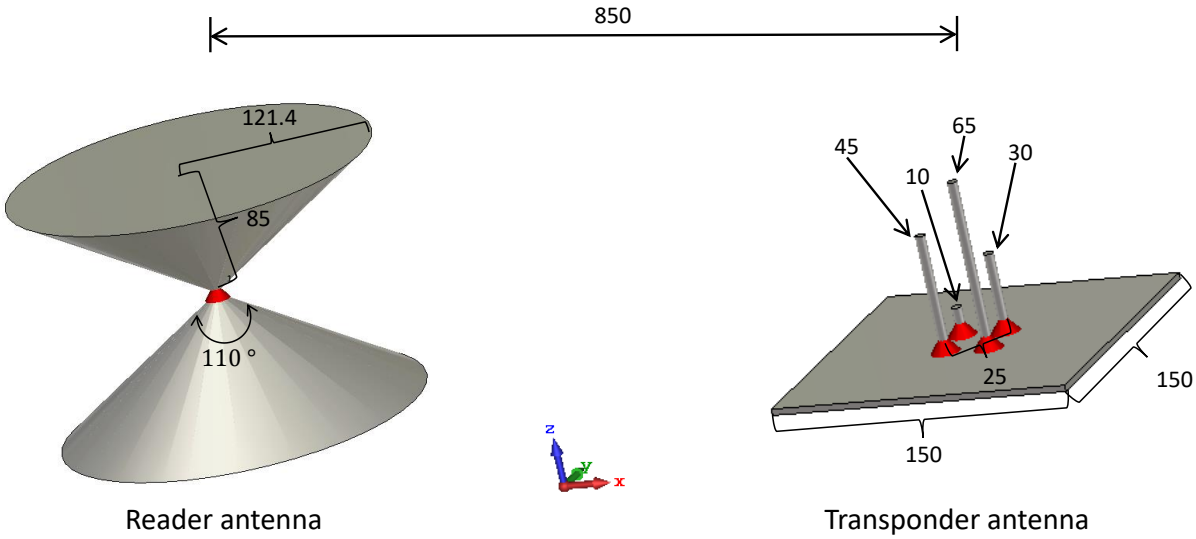

Fig. 11. The simulated antenna model used for the studied transponder. All the dimensions are in millimetres. The reader and transponder antennas are not in the real scale.

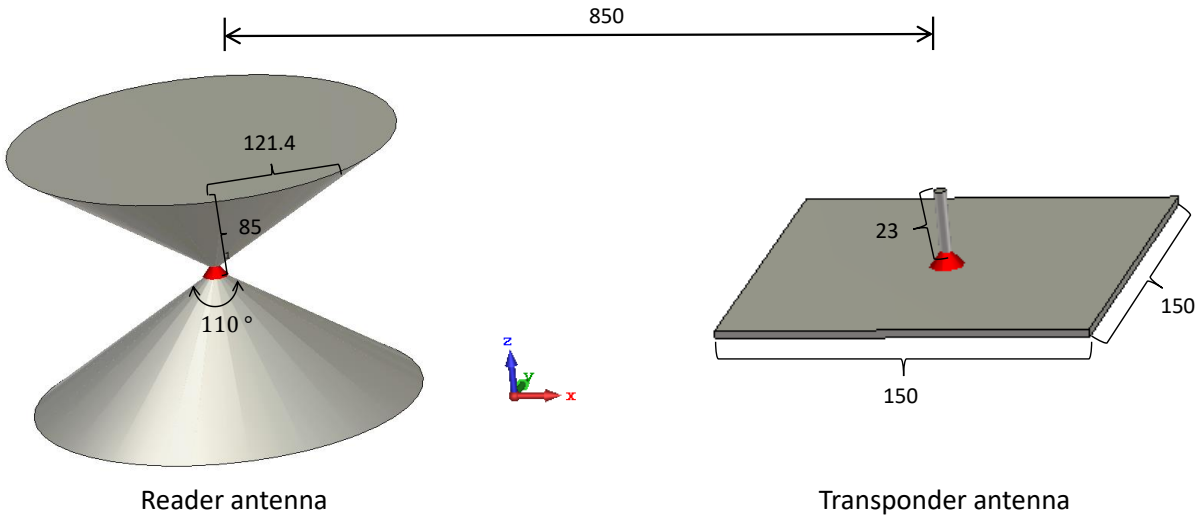

Fig. 12. The simulated antenna model used for the reference transponder. All the dimensions are in millimetres. The reader and transponder antennas are not in the real scale.

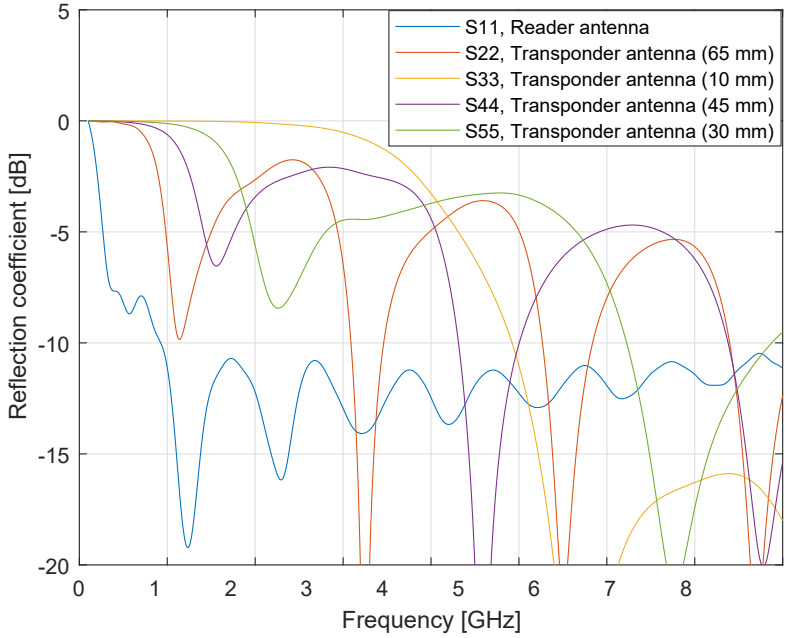

Fig. 13. The reflection coefficients of the antenna ports when the reference impedance is 50 ohms. Port 1 is reader antenna and Port 2, 3, 4 and 5 are the antenna elements of the studied transponder.

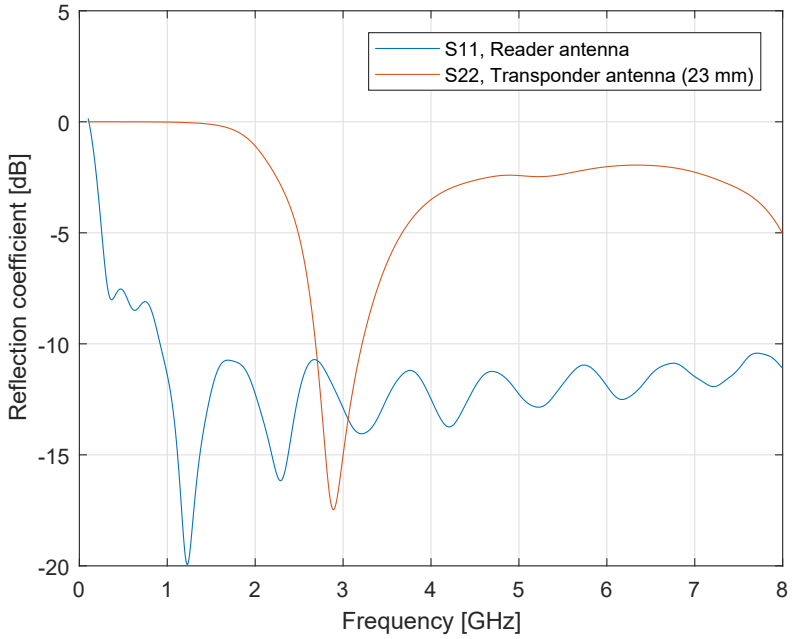

Fig. 14. The reflection coefficients of the antenna ports when the reference impedance is 50 ohms. Port 1 is reader antenna and Port 2 is the antenna element of the reference transponder.

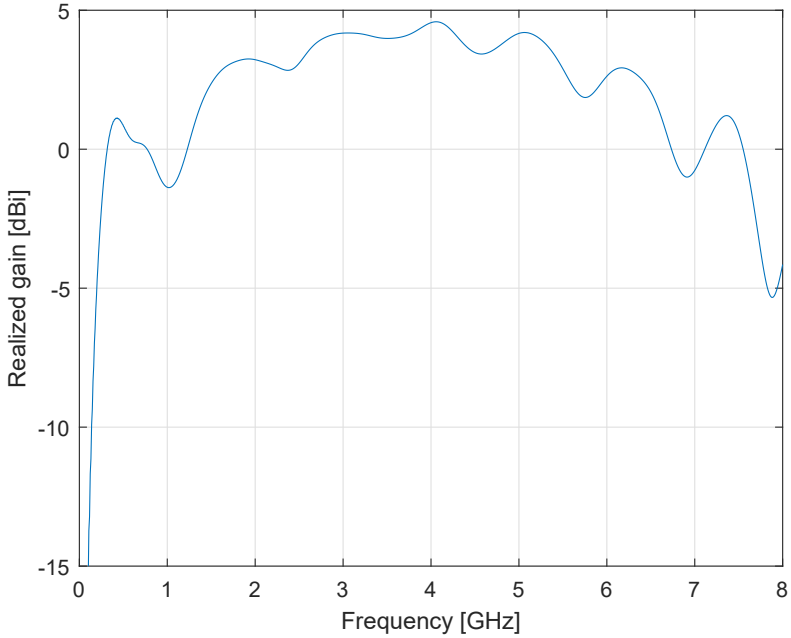

Fig. 15. The realized gain of the reader antenna in the direction of the transponder (i.e. $\theta = 90^o, \phi = 0^o$).

3.2 Mathematical model of the transponder

The scattering parameters of the studied transponder antenna (Fig. 11) was extracted from the CST Microwave Studio and modelled as 5 port network as shown in Fig. 16. The equivalent circuit of the reader and studied transponder are modelled as in Fig. 17.

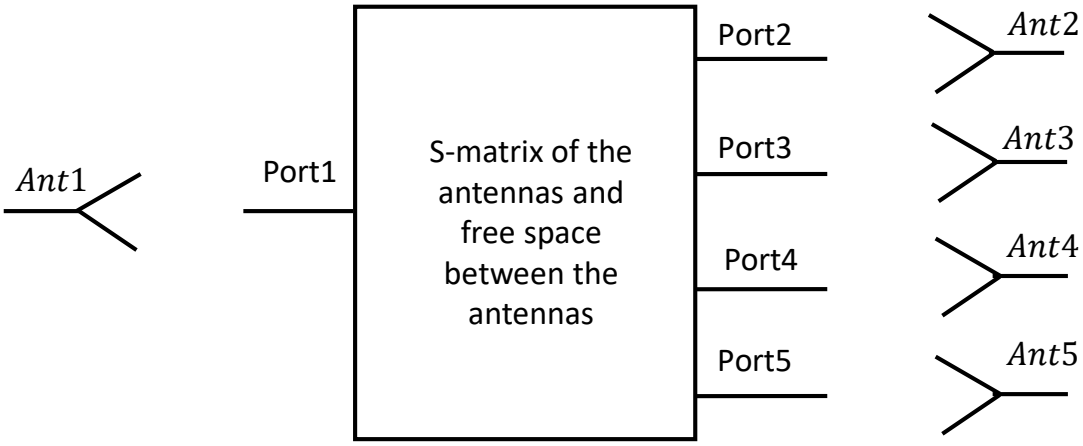

Fig. 16. The correspondence and notations of the antennas and the ports of the scattering matrix. Ant1 is the reader antenna and Ant2, 3, 4 and 5 are the antenna elements of the studied transponder.

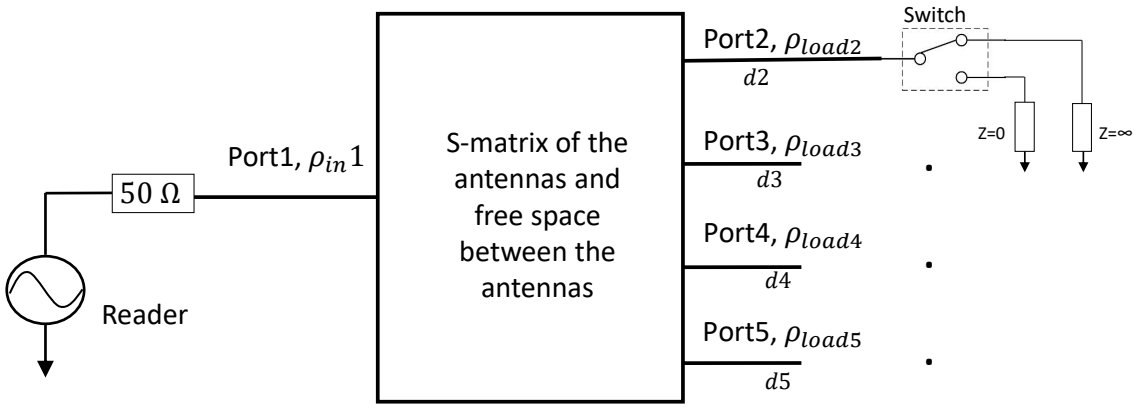

Fig. 17. The circuit model of the studied transponder. d2, d3, d4 and d5 are time domain delays as shown in Fig. 7 on the switch control signals of the modulators at Port 2, 3, 4 and 5 respectively.

In Fig. 16, the load impedance varies between the short and open circuits, and creates the modulated reflection coefficients ρ_{load2}, ρ_{load3}, ρ_{load4} and ρ_{load5} at Port 2, 3, 4 and 5 respectively. These reflection coefficients are calculated using Eq. (3). The switch connected to Port 2, switches with a reference square wave control signal voltage (i.e $d2 = 0$) and the switches connected to Ports 3, 4 and 5 switches with the delays of $d3$, $d4$ and $d5$ relative to the reference control signal respectively. The ρ_{in1} is the input reflection coefficient at Port 1.

The transponder models in Fig. 16 and 17 are similar to the N-port microwave network model, as shown in Fig. 10. Therefore Eq. (13) and (14) are used to calculate the input reflection coefficient at the reader antenna as:

$$\begin{vmatrix} S_{11}/\rho_{in1} - 1 & S_{21}/\rho_{in1} & \dots & S_{51}/\rho_{in1} \\ S_{12}\rho_{load2} & S_{22}\rho_{load2} - 1 & \dots & S_{52}\rho_{load2} \\ \vdots & \vdots & \ddots & \vdots \\ S_{1N}\rho_{load5} & S_{25}\rho_{load5} & \dots & S_{5}\rho_{load5} - 1 \end{vmatrix} = 0,$$

and

$$\rho_{in1} = \frac{S_{11}D_1 - S_{21}D_2 + S_{31}D_3 - ..... + S_{55}D_5}{D_1}. \tag{15}$$

As discussed in Section 2.5, the input reflection coefficient ρ_{in1} is the ratio of the reflected voltage wave to the incident voltage wave. Therefore, a modulated reflection coefficient $\delta\rho_{in1}$ would be defined as the ratio of the backscattered modulated voltage waves at modulated frequency $f_1 + f_m$ to the transmit voltage wave at frequency f_1. This means, if the reader transmit 0 dBm of power, it would receive $\delta\rho_{in1}$ dBm power at the modulated frequency from the transponder.

In the dB scale,

$$Received\ power\ at\ f_1 + f_m = \delta\rho_{in1} + transmit\ power. \tag{16}$$

The input reflection coefficient ρ_{in1} of Eq. (15) has components due to the modulated signal and S_{11} parameter. The S_{11} parameter is the reflection coefficient of the reader antenna and it must be subtracted from the input reflection coefficient to get the modulated reflection coefficient. Therefore, the modulated reflection coefficient ($\delta\rho_{in1}$) at Port 1 is:

$$\delta\rho_{in1} = \rho_{in1} - S_{11} = \frac{-S_{21}D_2 + S_{31}D_3 - ..... + S_{55}D_5}{D_1}. \tag{17}$$

Similarly, the modulated reflection coefficient $\delta\rho_{in1}$ of the reference antenna transponder can be modelled as a 2-port network. This gives:

$$\begin{vmatrix} S_{11}/\rho_{in1} - 1 & S_{21}/\rho_{in1} \\ S_{12}\rho_{load2} & S_{22}\rho_{load2} - 1 \end{vmatrix} = 0$$

or,

$$\rho_{in1} = S_{11} + \frac{S_{12}S_{21}\rho_{load2}}{1 - \rho_{load2}S_{22}},$$

and

$$\delta\rho_{in1} = \frac{S_{12}S_{21}\rho_{load2}}{1 - \rho_{load2}S_{22}}. \tag{18}$$

One of the main goals of this thesis is to study if, one can optimize the phases (i.e. time domain delays) of the modulators of the studied transponder in such a manner, that its backscattered signal power is maximized or at least larger than the backscattered power of the studied transponder when the phases of the modulators are zeros (i.e. $d = 0$), and compare the results with that of the reference transponder.

It is good to note from Eq. (3) and (17) that the modulated reflection coefficient $\delta\rho_{in1}$ is a function of the time domain delay d of the switch control signal at the different modulators. Also, from Eq. (5) note that a time domain delay gives a phase difference in the frequency domain. Therefore, using time domain delays in the switch control signals gives phase variable modulators.

The switch control signal of the modulator at Port 2 is taken as a reference, and the switch control signals of the modulators at Port 3, 4 and 5 are delayed with respect to the reference. In this case, delay $d = 0$ for ρ_{load2}, and optimal delay values $d3$, $d4$ and $d5$ for ρ_{load3}, ρ_{load4} and ρ_{load5} respectively are used to maximize the modulated reflection coefficient (i.e. the received modulated power when the transmit power is 0 dBm). The reference transponder is modelled using the switch control signal with delay $d = 0$ for its modulator. The reference modulator have single modulator, therefore, the delay value is senseless.

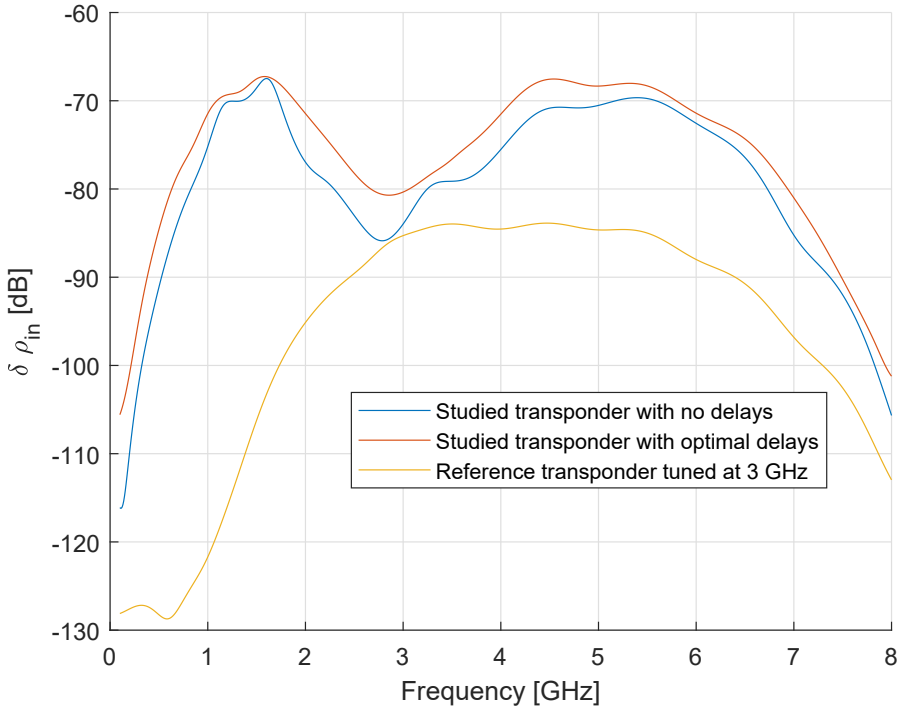

Fig. 18. The modulated reflection coefficients of the studied and reference antenna transponders.

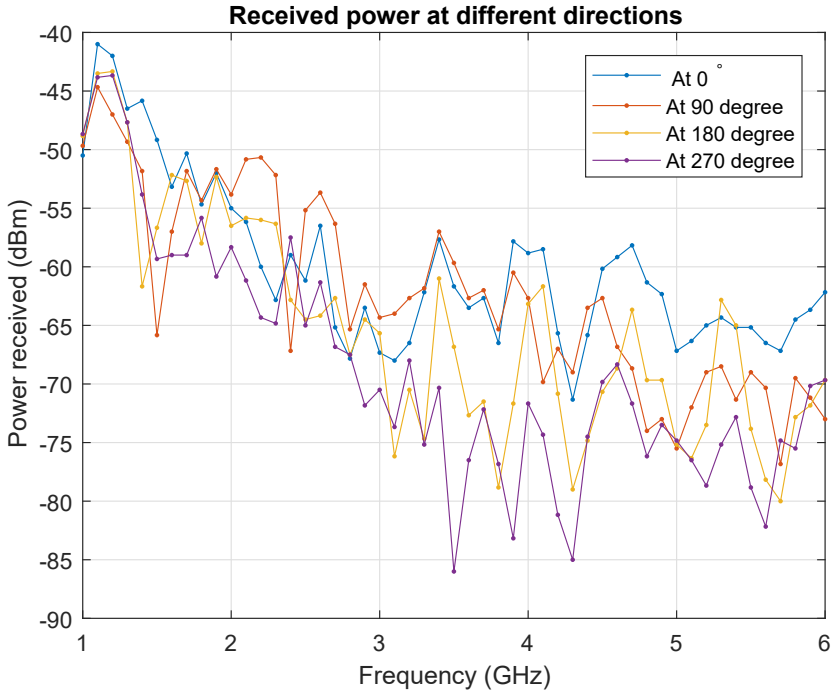

Fig. 19. The modulated reflection coefficients of the studied transponder at different directions, when there are no delays in the switch control signals.

The modulated reflection coefficients for the studied and reference transponders were simulated in Matlab using Eq. (17) and (18) respectively. The delay values of Eq. (17) were optimized using Mathematica [29] to maximize the modulated reflection coefficient $\delta\rho_{in1}$. The result of the simulation is shown in Fig. 18. The Fig. 18 shows the received power at frequency $f_1 + f_m$ at the reader antenna when the transmitted power at frequency f_1 is 0 dBm. This is the main result of this thesis work. The orientation of the transponder antenna as shown in Fig. 11 is taken as 0 degree, and the modulated reflection coefficient of the studied transponder in the directions 0, 90, 180 and 270 degrees are simulated. The results of the simulation are shown in Fig. 19. The results obtained in this section are analysed at the end of this chapter (in Section 3.3).

3.3 AWR simulation of the transponder

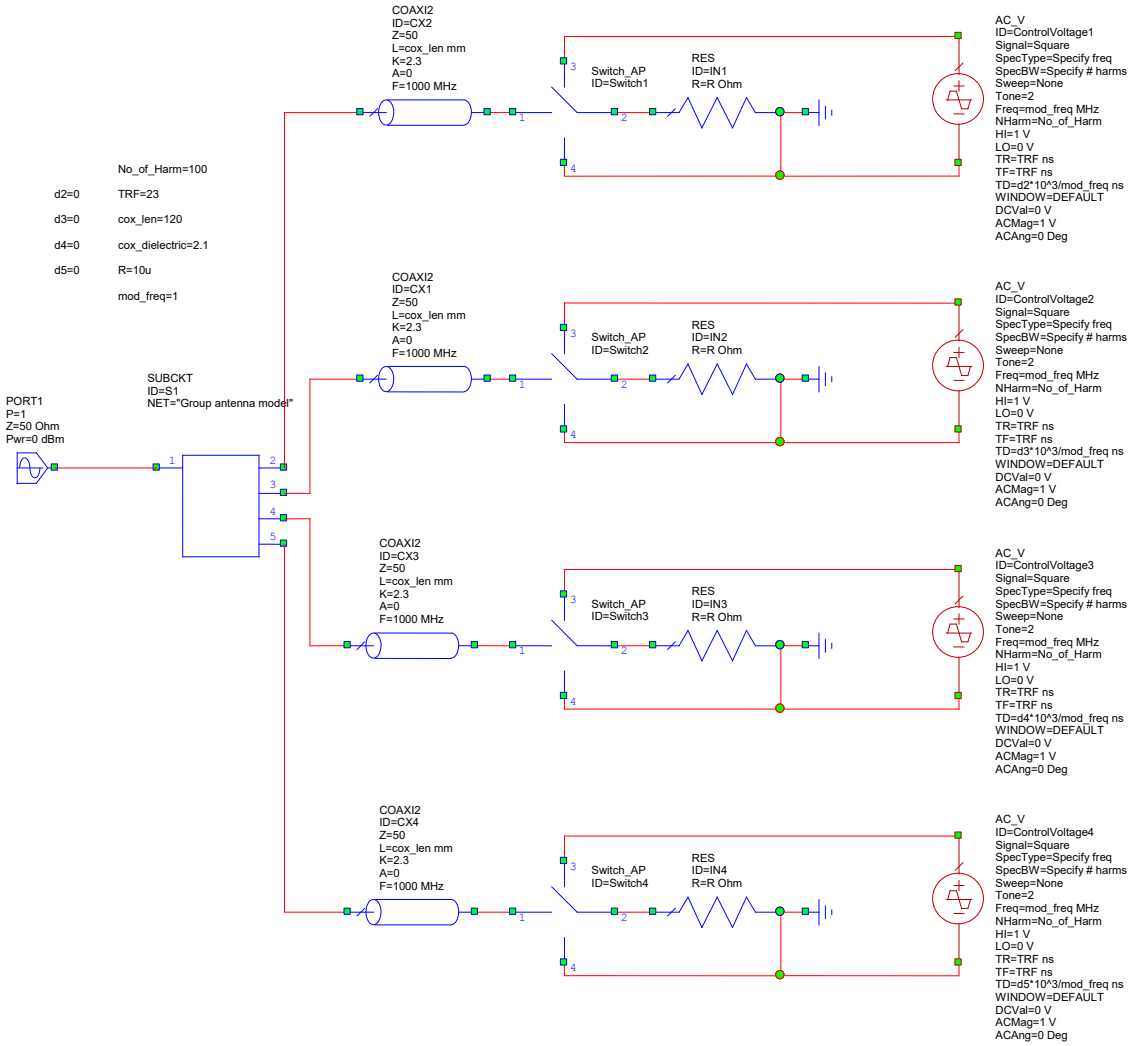

Fig. 20. The AWR circuit diagram for the studied transponder.

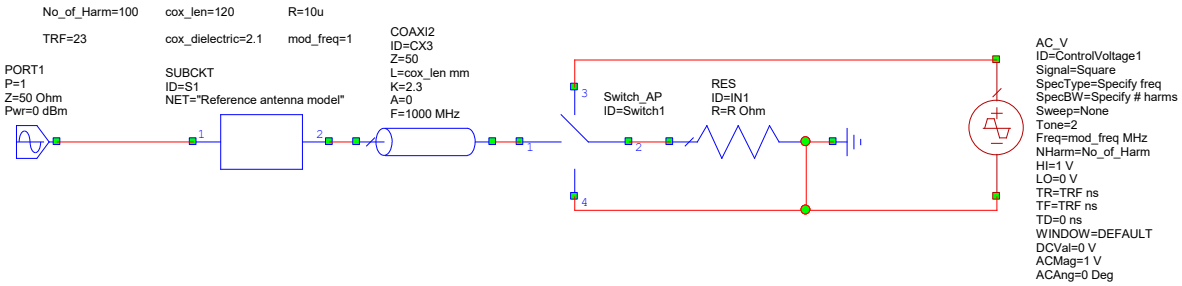

Fig. 21. The AWR circuit diagram for the reference transponder.

The operations of the transponders were also studied using AWR Microwave Office circuit simulator [27]. The schematic models used in AWR simulations are shown in Fig. 20 and 21. Port 1 is excited with a signal at frequency f_1 with 0 dBm power, and the power at first harmonics $f_1 + f_m$ at Port 1 was simulated. The AWR circuit models are the same as that used in Matlab simulations in Section 3.2, Fig. 17.

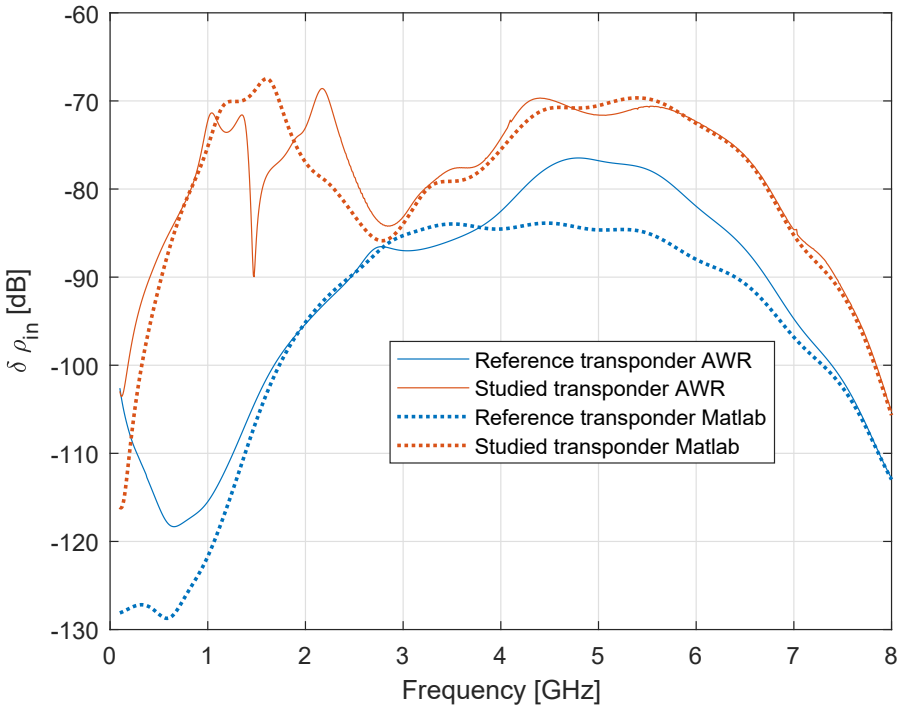

Fig. 22. The modulated reflection coefficient based on AWR and Matlab simulations.

The solver used in the AWR simulations is APLAC harmonic balance (HB) circuit simulation engine [30]. Fig. 22 shows that the results of AWR and Matlab simulations are matched quite well, with some exceptions. The simulation done in Matlab assumes

that the switches are ideal and they are switching infinity fast. In AWR, these ideal switches make the circuit strongly non-linear for APLAC HB simulator and APLAC HB fails to converge the results accurately at certain frequencies. This is why there is the difference in results of Matlab and AWR simulations [30].

3.4 Analysis of the results

The Eq. 1 shows that the power received by the reader is directly proportional to the gain of the reader antenna and the operating frequency. Therefore the modulated reflection coefficient $\delta\rho_{in1}$ of Fig. 18 is shaped by the realized gain of the reader antenna, as shown in Fig. 15, and the operating frequency is determined by the S_{11} parameters of each monopole antenna elements of the transponder antennas, as shown in Fig. 13 and 14.

The modulated reflection coefficient of the reference transponder near 3 GHz is large because its antenna is tuned near 3 GHz. However, it is large also at 4, 5 and 6 GHz, because the antenna element has sufficiently good matching at these frequencies (see Fig. 14). The studied antenna has multiple antenna elements and its operational band is distributed across 1-6 GHz. Therefore, the received power of the studied transponder is higher than that of the reference transponder. In the best case at 1 GHz, it is even up to 40 dB higher. It is good to note that the modulated received power is decreasing as frequency increases. This is because when the frequency increases, the effective aperture of the antenna decreases, which reduces the received power as in Eq. (1), if the antenna gains are constant.

The result based on AWR simulations in Fig. 22 also supports these observations and provides more evidence that the mathematical models of the transponders, developed in this thesis are valid. These results clearly show that the operating range of the studied transponder is much wider than that of the reference transponder. Also from Fig. 19, it can be observed that the modulated reflection coefficient of the studied transponder is not the same in all direction. This means the transponder is not fully omnidirectional.

Furthermore, the received power can be increased by using optimal delay values (see Fig. 18). These optimal delay values change as a function of frequency, and in the best case (e.g. at 2.8 GHz), the received power increases even up to 10 dB. This means that the feasibility of increasing the received power of a transponder based on coupled antenna elements and phased modulators by changing phases of the incident signals of antenna elements is positive. These results are based on the simple antenna models as shown in Fig. 11 and 12. It is possible to improve the performance of the transponder by further optimizing the antenna structure.

4 Measured transponder model and results

After the simulations, a prototype reference and a prototype studied transponders/demonstrators were built, and their behaviours were studied, in a real environment through measurements. This chapter, first briefly discusses, how the prototypes were built. Then it shows the measurement setup and the measurement results. At the end of this chapter, the measurement results are analysed and compared with the simulation results discussed in Chapter 3.

4.1 Prototype transponder

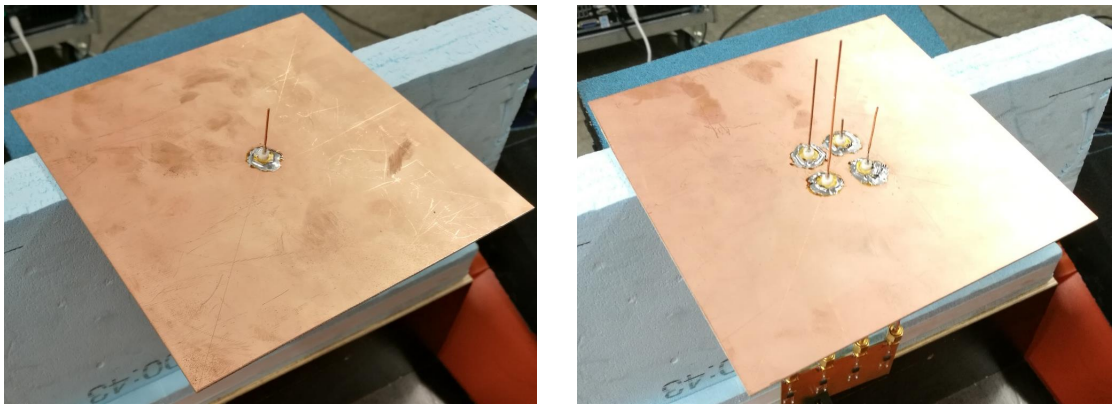

Fig. 23. Antennas for the prototype transponders. a) Reference transponder antenna. b) Studied transponder antenna. The dimensions are the same as in Fig. 11 and 12.

Based on the simulation results, prototype transponders were built in order to demonstrate their behaviour in the real environment. The prototype transponder antennas are shown in Fig. 23. The dimensions of these antennas are shown in Fig. 11 and 12.

The modulators were implemented on a printed circuit board (PCB) as shown in Fig. 24. It was designed using PADS circuit designer [31] and manufactured using a vendor called Eurocircuits [32]. The input and outputs of the switches are connected to DC block capacitors of 47pF. The switches inputs RF-COM are connected through an SMA connector to the antenna elements of the transponder. The outputs RF2 are connected to 2 $M\Omega$ resistors for high impedance termination (open circuit), and the outputs RF1 are connected directly to the ground for low impedance termination (short circuit). They are powered with 3.8 V DC and the switch control voltages are the square waveform of 3.3 V for high and 0 V for low. The switches are SPDT RF switch (VSWA2-63DR+) from Mini-Circuits [33]. The capacitors and resistors were from Murata [34].

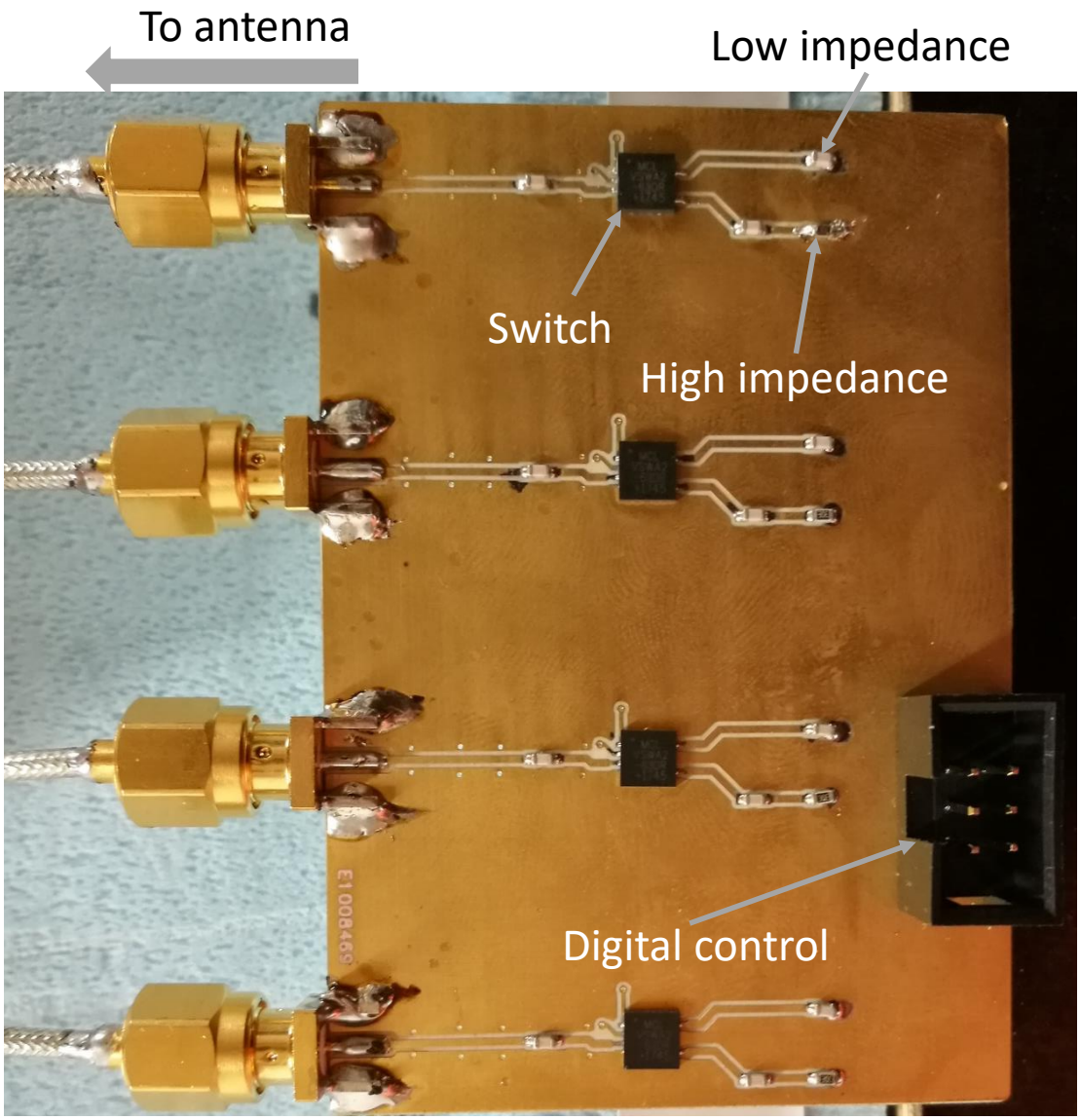

Fig. 24. The printed circuit board of the modulator circuit.

The reflection coefficient for ideally short-circuited antenna element ρ_1 is -1, and reflection coefficient for ideally open-circuited antenna element ρ_2 is +1. From Eq. (4), (13) and (17), it can be seen that the modulated reflection coefficient $\delta\rho_{in1}$ at the reader antenna (the received power at the modulated frequency $f_1 + f_m$, when transmit power is 0 dBm) is directly proportional to the change in reflection coefficients of open-circuited and short-circuited load impedances (i.e. $\delta\rho_{in1} \propto |\rho_1 - \rho_2|$).

For ideal short and open circuit terminations, change in the reflection coefficient $|\delta\rho| = |\rho_1 - \rho_2| = 2$. However in a real environment, ideal short and open circuit terminations in microwave frequencies are very hard to achieve. Therefore, in the real environment $|\delta\rho|$ is less than 2. The reflection coefficients of the modulator

PCB during the short circuit and open circuit were measured using a vector network analyzer [35]. Fig. 25 shows change in the measured reflection coefficient. $|\delta\rho|$ of the modulators at Port 2, 3 4 and 5 are very similar, and they are quite big across the desired frequency range. These results show that the modulator circuit is performing sufficiently good.

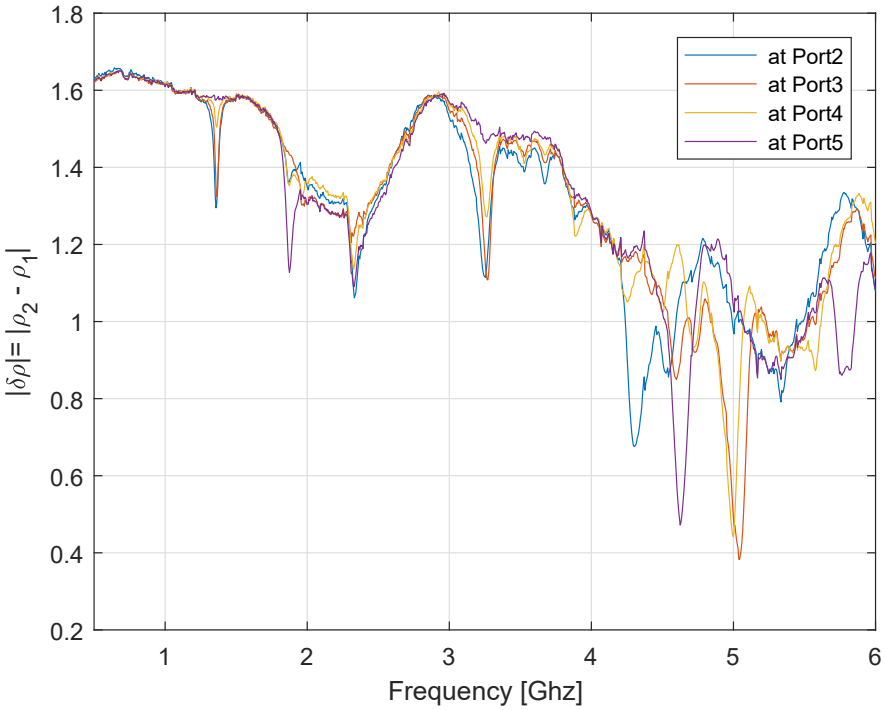

Fig. 25. Change in reflection coefficients due to the short and open circuit in the modulators at different ports.

4.2 Measurement set up

Fig. 26 shows the block diagram of the measurement setup, and Fig. 27 shows the anechoic (measurement) chamber of Aalto University, School of Electrical Engineering. The reader consists of a signal generator [36], two Vivaldi antennas [37], and a spectrum analyser [38]. The transponder consists of the transponder antenna, modulators, a logic analyser [39] and a DC power supply.

The signal generator provides an RF signal of 24 dBm power at a frequency range of 1-6 GHz. The signal generator is connected to a Vivaldi antenna by an 0.5 meters RG-58 coaxial cable. The Vivaldi antenna transmits the RF signal to the transponder, which is located 1.6 meters away. The logic analyser creates the necessary switch control signals for the modulators in the transponder. The rise and fall times of the RF switches are 23 ns [33]. The logic analyser produces square wave signals of 1 MHz whose rise and fall times are 5 ns, which are smaller than

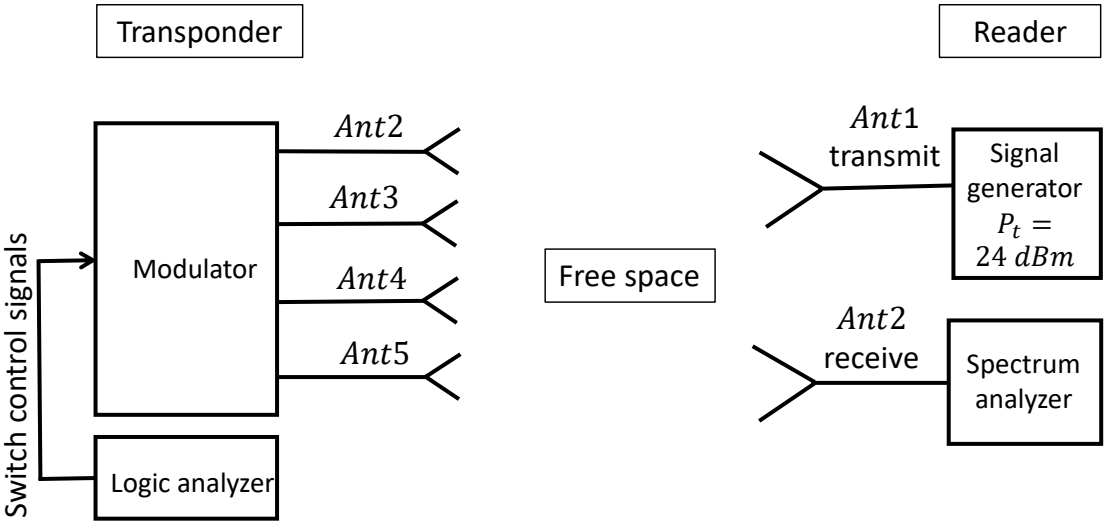

Fig. 26. The block diagram of the measurement setup.

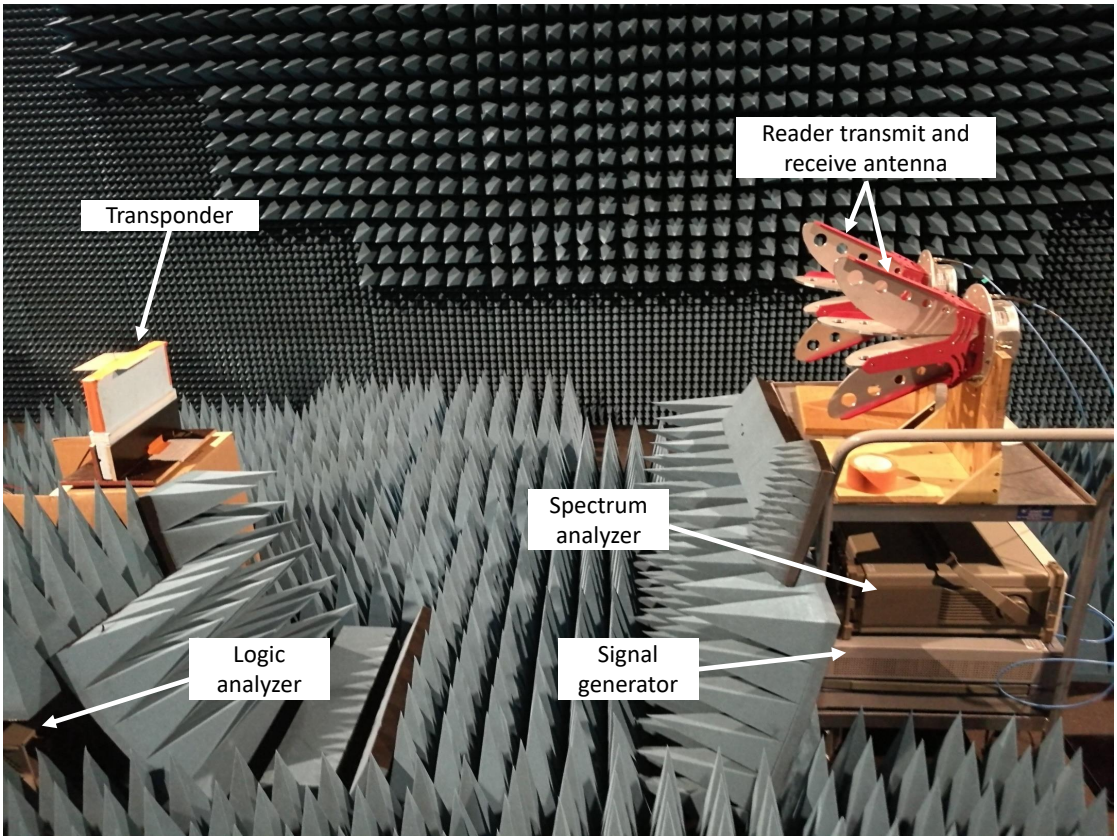

Fig. 27. The measurement setup in the anechoic chamber at Aalto University.

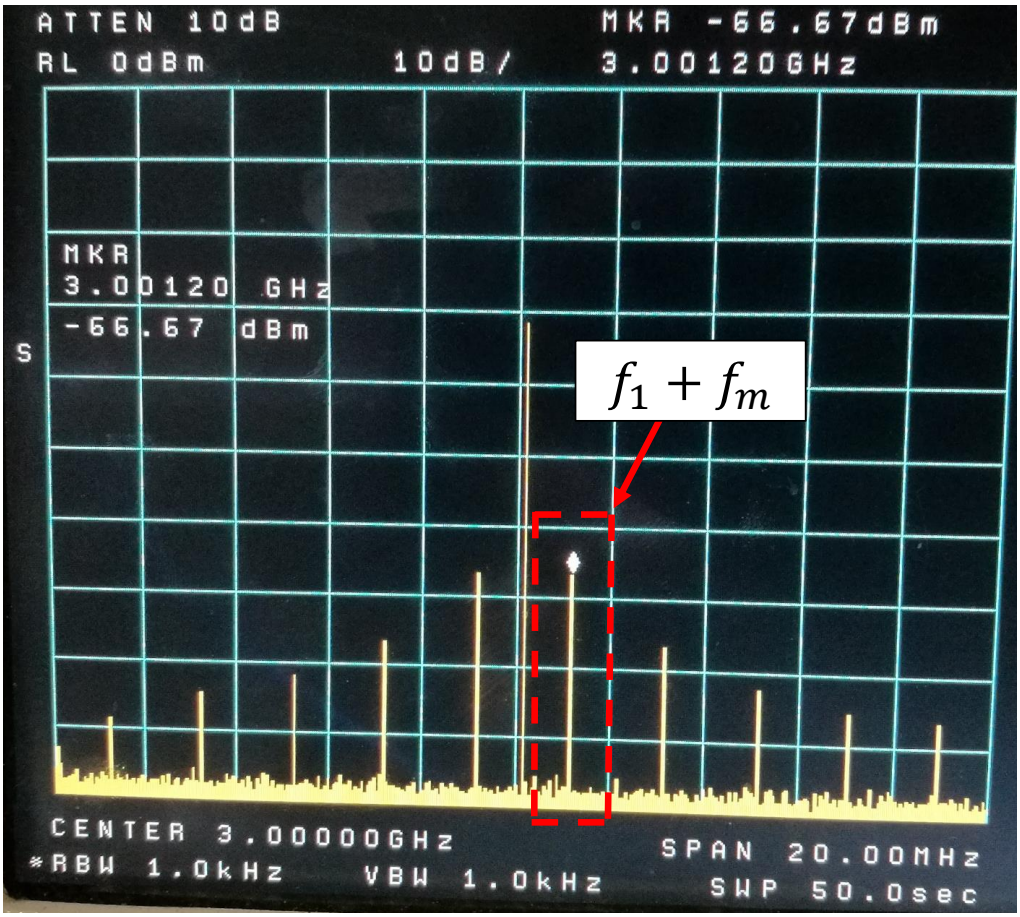

Fig. 28. The frequency spectrum of the received power seen in the spectrum analyser.

that of the RF switches used in the modulators. Therefore the square wave signals generated by the logic analyser are sufficiently good for this application. The square waves have 3.3 V for high and 0 V for low. The logic analyser has generated four switch control signals for four modulators, which could be delayed by the resolution of 100 ns. The DC power supply provides a 3.8 V DC for the RF switches.

The transponder receives the signal transmitted by the reader and backscatters a modulated signal. The modulated signal is received by the reader through another Vivaldi antenna and it is measured with a spectrum analyser. The Vivaldi antenna and spectrum analyser are also connected by an RG-58 coaxial cable of 0.5 meters.

In Section 2.4, it was discussed that the Fourier series of a square wave has the odd number of harmonics (see Fig. 6). The modulators modulate the incoming signals with a switch control signal (which is a square wave) and produce a modulated signal which has frequency components in the odd number of harmonics. Therefore, the received backscattered power should have the signal with frequency components in the odd numbers. This is verified in Fig. 28, which is the frequency spectrum of

the received power seen in the spectrum analyser. It shows that the received power indeed has the frequency components in the odd number of harmonics. It is good to note that in Fig. 28, the strongest signal is at the transmit frequency f_1. This signal is seen, because of the coupling between two Vivaldi antennas and in lesser extent due to reflections on measurement environment. In measurements, the power level at the first harmonics of the received power is measured and studied.

4.3 Measurement results

The measurement results and their analyses are presented in this section. The setup during the simulations in Chapter 3 and the setup during the measurements, in this chapter are not the same. The main difference is that in simulations, the distance between the reader and transponder was 0.85 m and the reader antenna was a single finite biconical antenna, which transmits and receives the RF signals, whereas in the measurements the distance between the reader and transponder was 1.6 m and there were two Vivaldi antennas, each for transmitting and receiving the RF signals. Therefore one can not compare simulations and measurements results directly. However, the prototype transponders are the same in both the simulations and measurements, as modelled in Chapter 3. Hence, even if the received power levels are different, the general shape of the curves should be comparable.

The received power of the reference and studied transponders without delays is shown in Fig. 29. It is good to note that in Fig. 29, the measured power has lots of fluctuations as a function of frequency. The transponder load impedance modulates between short and open circuits, and it produces reflections of reflection coefficients -1 and +1 respectively. When a connecting cable is used between the modulators and antenna elements, these reflections create standing waves in the cable. The physical length of the cable is fixed, and its electrical length changes depending on the operating frequency. The antenna elements would see different parts of standing waves at different frequencies. These waves will constructively or destructively superpose each other and produce fluctuations in the received power. Therefore the measured results as in Fig. 29 have fluctuations.

The results of AWR simulations performed with and without 12 cm 50 ohms, coaxial cables, which connect the antenna elements to the modulators are shown in Fig. 30. In this figure, it is clearly seen that the case without the connecting cables has smooth curves, whereas, the case with the connecting cables has lots of fluctuations. These results verify that the fluctuations seen in the measurement results are because of connecting cables, which are used to connect the outputs of the modulators to the inputs of the antenna elements.

It is good to note that in Fig. 29, the studied transponder performed better than the reference transponder except at 3 GHz. The reference transponder is tuned at 3 GHz, and it performed best at 3 GHz. The studied transponder performed up to 40 dB better than the reference transponder for instance at 1.1 GHz. These observations

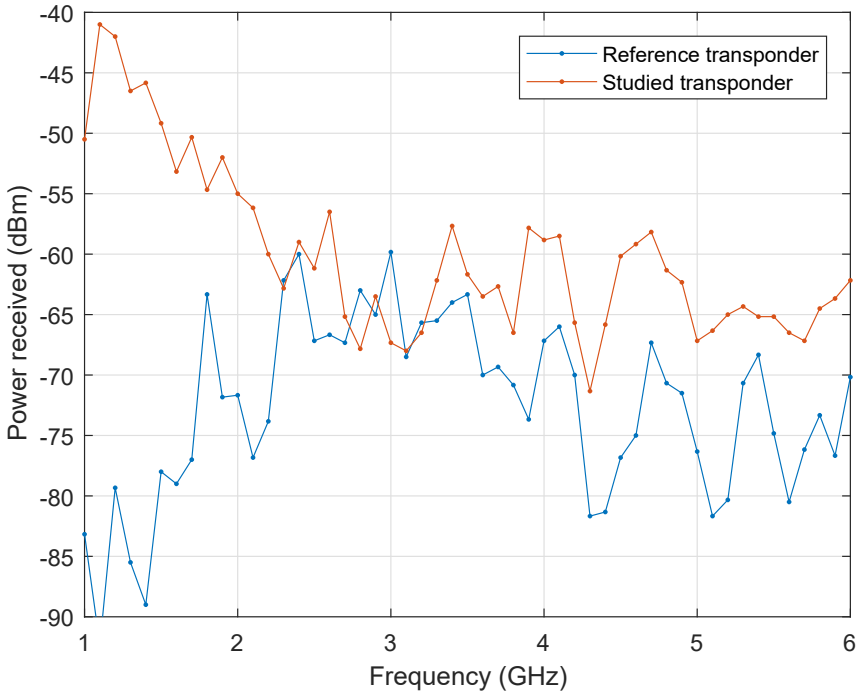

Fig. 29. The received power from the reference and studied transponders without delays during measurements.

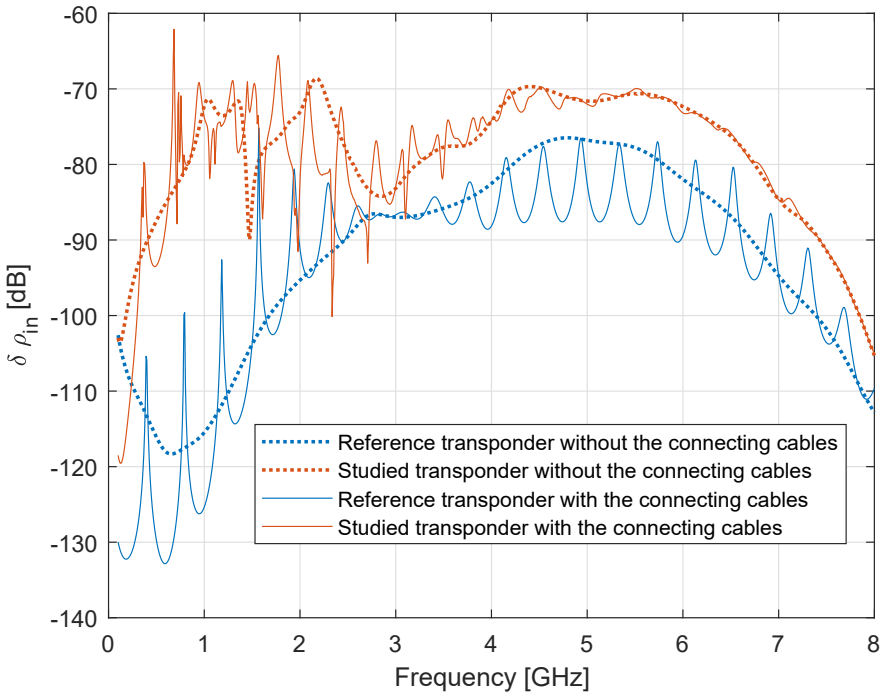

Fig. 30. The modulated reflection coefficients with and without the connecting cables based on AWR simulations.

are similar to the observations observed during simulations in Section 3.4, Fig. 18.

When 1 MHz switch control signal is delayed with a resolution of 100 ns, there are 10 different possible delay values. When the switch control signal (of 1 MHz) of the modulator connected to Port 2 is taken as the reference and the switch control signals of the modulators connected to Port 3, 4 and 5 are delayed with the resolution of 100 ns, there are 1000 different combinations of delay values. In this thesis, the measurements are done manually, and going through all 1000 different combinations are impractical. Therefore, a sample of five random different delay values is selected, and the measurements are done with these five different samples of delay values.

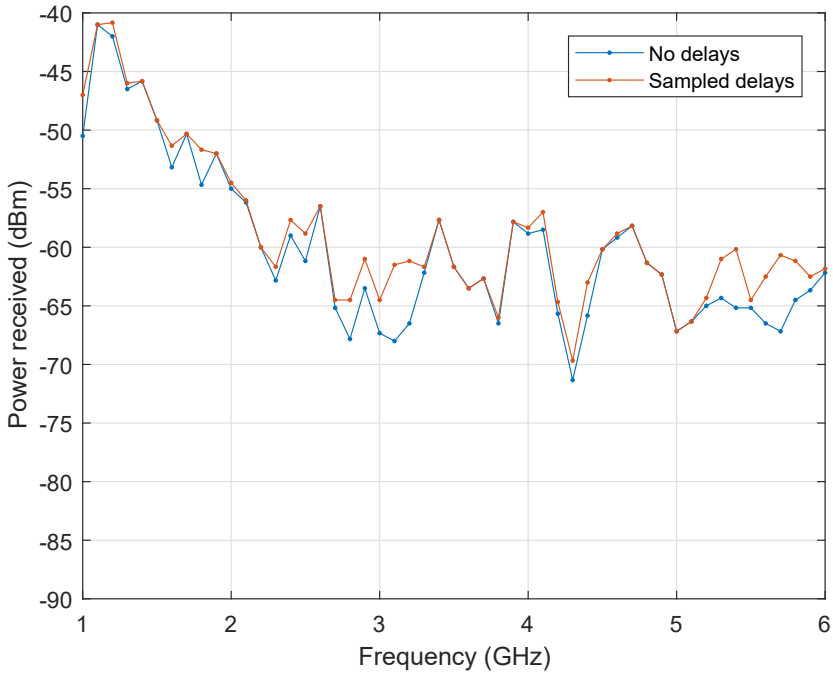

Fig. 31. The received power without delays, and the maximum received power with the sampled delays from studied transponder during measurements.

Fig. 31 shows the received power of the studied transponder when there are no delays and that of the sampled delays. The received power of sampled delays is the best (i.e. maximum received power) of the 5 selected samples at each frequency. Fig. 31 shows that even with just 5 random samples, the received power of the studied transponder has increased by 6 dB at some frequencies. The measurement uncertainty of the measurement caused by the measurement equipment is around ±2 dB. Since the improvement in the performance of the transponder with the sampled delays is higher than the measurement uncertainty, one can conclude that it is possible to increase the performance of the transponder by optimizing the phases of the modulators compared to the constant phase modulators. It is good to notice that

these observations are also similar to the observations observed during simulations in Section 3.2, Fig. 18.

The performance of the studied transponder is also measured at different directions. The orientation of the transponder antenna as shown in Fig. 11 is taken as 0 degrees, and the received power measured at 0 degrees, 90 degrees, 180 degrees and 270 degrees are shown in Fig. 32. These results also show that the transponder is not fully omnidirectional. These observations are also similar to the observations observed during simulations in Section 3.2, Fig. 19.

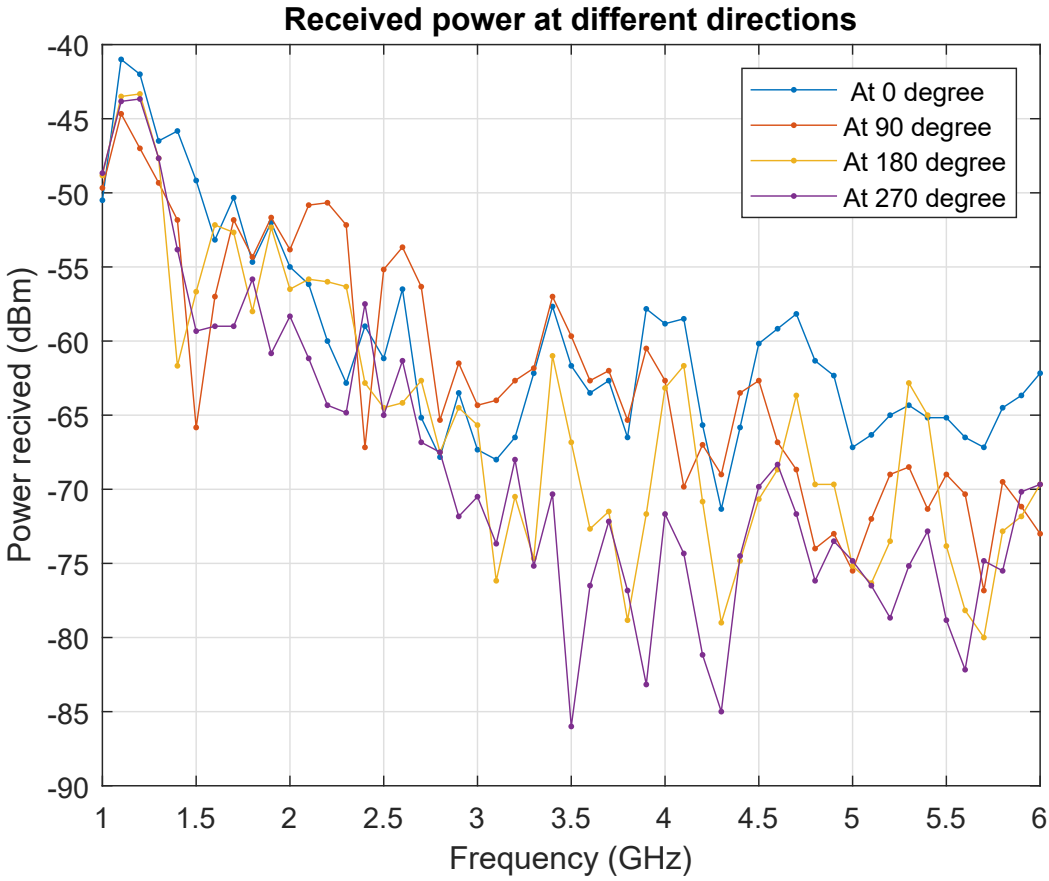

Fig. 32. The received power of the studied transponder without delays from different directions.

5 Conclusion

In this thesis, a broadband transponder based on coupled antenna elements and phased modulators were studied, and its performance was compared with a reference transponder based on a single antenna element and a single modulator. First, the transponders were mathematically modelled and their performances were studied through computer simulations. Then the transponders were prototyped/demonstrated and their performances were studied through measurements.

In both simulations and measurements, it was found that the studied transponder without the phased modulators performed better than the reference transponder over a frequency range of 1-6 GHz (see Fig. 18 and 29). The studied transponder performed up to 40 dB higher at certain frequencies (e.g. at 1 GHz) compared with the reference transponder in both simulations as well as in measurements.

In addition to this, the performance of the studied transponder based on the optimally phased modulators was further increased up to 10 dB at certain frequencies in simulations (see Fig. 18), compared with the studied transponder based on constant phase modulators. In measurements, it was impractical to go through all the combinations of delay values (phases) of the modulators manually, therefore, the received power at modulated frequency $f_1 + f_m$ was measured for only five random samples of delay values. Even with these five randomly sampled delay values, it was found that the performance of the studied transponder based on sampled phased modulators increased up to 6 dB at certain frequencies, compared with the studied transponder based on constant phase modulators (see Fig. 31).

The measurements were done manually, therefore, it was impossible to go through all the combinations of the delay values. If this topic is studied further, one could automate the measurement setup such that it will go through all the possible delay values, and find the optimal delays, which would maximize the received power of the studied transponder based on optimally phased modulators.

In addition to this, the received power can further be improved by optimizing the antenna structure. One can also, build the same simulation and measurement models such that their results can be compared directly which might help to study the topic further. The mathematical model of the transponders in this thesis depends upon the scattering parameters of the reader antenna (see Chapter 3). This model is not always convenient. A better model might be if the mathematical model is independent of the scattering parameters of the reader antenna. Therefore, one can revisit the theories and concepts, and build a new mathematical model for the transponder.

As discussed in Section 2.3, the constant amplitude, optimally phased input signals at the antenna elements of a strongly coupled antenna cluster might improve the matching efficiency of the studied transponder, compared with the constant

amplitude constant phase input signals. The antenna structure with a good matching efficiency increases the performance of the transponder. However, the phased inputs also, steer the beam of the radiation pattern of an antenna array [40]. In this thesis, it is not studied whether the increase in the performance of the studied transponder based on the phased modulators compared with that of constant phase modulators, was solely because of improvement in matching efficiency of the antenna cluster, solely because of the beam steering like in conventional to phased antenna array or a combination of these two concepts. This topic should be further studied. If the increase in the performance of the studied transponder is because of the combination of beam steering as well as improvement in matching coefficient, then it will open new possibilities like a broadband beam steerable transponders, which might be used in future IoT applications.

References

[1] Oxford University Press, *Oxford dictionaries*. [Online]. Available at https://en.oxforddictionaries.com/definition/transponder, (cited: 27.06.2018).

[2] K. Finkenzeller, *RFID Handbook, 3rd Edition*. Wiley, 2010.

[3] K. Sohraby, D. Minoli, and T. Znati, *Wireless Sensor Networks*, ch. 1 Introduction and Overview of Wireless Sensor Networks, pp. 1–37. Wiley, 2007.

[4] M. Kusek, "Internet of things: Today and tomorrow," in *2018 41st International Convention on Information and Communication Technology, Electronics and Microelectronics (MIPRO)*, pp. 0335–0338, May 2018.

[5] M. P. Singh and A. K. Chopra, "The internet of things and multiagent systems: Decentralized intelligence in distributed computing," in *2017 IEEE 37th International Conference on Distributed Computing Systems (ICDCS)*, pp. 1738–1747, June 2017.

[6] N. V. Huynh, D. T. Hoang, X. Lu, D. Niyato, P. Wang, and D. I. Kim, "Ambient backscatter communications: A contemporary survey," *IEEE Communications Surveys Tutorials*, pp. 1–1, 2018.

[7] R. M. C. Cleetus and G. J. Bala, "Frequency reconfigurable antennas: A review," in *2017 International Conference on Signal Processing and Communication (ICSPC)*, pp. 160–164, July 2017.

[8] J. M. Hannula, J. Holopainen, and V. Viikari, "Concept for frequency-reconfigurable antenna based on distributed transceivers," *IEEE Antennas and Wireless Propagation Letters*, vol. 16, pp. 764–767, 2017.

[9] R. M. White, "A sensor classification scheme," *IEEE Transactions on Ultrasonics, Ferroelectrics, and Frequency Control*, vol. 34, pp. 124–126, March 1987.

[10] "IEEE Standard for Sensor Performance Parameter Definitions," *IEEE Std 2700-2014*, pp. 1–69, Aug 2014.

[11] D. Culler, D. Estrin, and M. Srivastava, "Guest editors' introduction: Overview of sensor networks," *Computer*, vol. 37, pp. 41–49, Aug 2004.

[12] A. Ahmed, J. Ali, A. Raza, and G. Abbas, "Wired vs wireless deployment support for wireless sensor networks," in *TENCON 2006 - 2006 IEEE Region 10 Conference*, pp. 1–3, Nov 2006.

[13] I. F. Akyildiz, W. Su, Y. Sankarasubramaniam, and E. Cayirci, "A survey on sensor networks," *IEEE Communications Magazine*, vol. 40, pp. 102–114, Aug 2002.

[14] H. H. Khalili, P. R. Green, D. George, G. Watson, and W. Schiffers, "Wireless sensor networks for monitoring gas turbine engines during development," in *2017 IEEE Symposium on Computers and Communications (ISCC)*, pp. 1325–1331, July 2017.

[15] M. Youssef and N. El-Sheimy, "Wireless sensor network: Research vs. reality design and deployment issues," in *Fifth Annual Conference on Communication Networks and Services Research (CNSR '07)*, pp. 8–9, May 2007.

[16] O. Olorunniwo, L. O. Kehinde, and M. A. Olorunniwo, "Global wsn developments: Fractal or chaos?," in *Proceedings of PICMET '14 Conference: Portland International Center for Management of Engineering and Technology; Infrastructure and Service Integration*, pp. 609–619, July 2014.

[17] ON World Inc, *Wireless Sensor Network Markets*, May 2018. [Online]. Available at https://www.researchandmarkets.com/research/km53jd/global_wireless?w=4, (cited: 27.06.2018).

[18] "IEEE Standard Definitions of Terms for Antennas," *IEEE No 145-1973*, pp. 1–18, Aug 1973.

[19] A. F. Molisch, *Wireless Communications, 2nd Edition*, ch. 4.1 Free Space Attenuation, p. 47. Wiley, 2011.

[20] D. Pozar, *Microwave Engineering, 4th Edition*. Wiley, 2011.

[21] R. C. Hansen, "Correct impedance-matching limitations [antenna designer's notebook]," *IEEE Antennas and Propagation Magazine*, vol. 51, pp. 122–124, June 2009.

[22] G. B. Arfken and H. J. Weber, *Mathematical Methods For Physicists International Student Edition, 6th Edition*, ch. 14, Fourier series, p. 881. Elsevier Academic Press, 2005.

[23] V. Teppati, A. Ferrero, and M. Sayed, *Modern RF and Microwave Measurement Techniques*, ch. 1.3 Scattering Parameters, p. 47. Cambridge University Press, 2013.

[24] J. X. Yun and R. G. Vaughan, "A view of the input reflection coefficient of the n-port network model for mimo antennas," in *2011 IEEE International Symposium on Antennas and Propagation (APSURSI)*, pp. 297–300, July 2011.

[25] Dassault systems, *Computer Simulated Techolology (CST) Microwave Studio 2017*. [Online]. Available at https://www.cst.com/products/csts2, (cited: 27.06.2018).

[26] MathWorks, *Matlab R2017b*. [Online]. Available at https://se.mathworks.com/products/matlab.html, (cited: 27.06.2018).

[27] National Instruments, *AWR design environment 13.* [Online]. Available at http://www.awrcorp.com/products/ni-awr-design-environment/microwave-office, (cited: 27.06.2018).

[28] W. L. Stutzman and G. A. Thiele, *Antenna theory and design, 3rd Edition*, ch. 7.4 Biconical antenna, pp. 233–239. Wiley, 2012.

[29] Wolfarm Research, *Wolfarm Mathematica 11.* [Online]. Available at http://www.wolfram.com/mathematica/, (cited: 27.06.2018).

[30] National Instruments, *Simulation and Analysis Guide NI AWR Design Environment v13.03 Edition*, ch. 6 Harmonic balance analysis.

[31] Mentor Graphics, *PADS logic and PADS layout.* [Online]. Available at https://www.pads.com/, (cited: 27.06.2018).

[32] Eurocircuits, *PCB manufacturer.* [Online]. Available at https://www.eurocircuits.com/pcb-prototype-and-small-series-services-offered-by-eurocircuits-made-in-euro (cited: 27.06.2018).

[33] Mini-Circuits, *SPDT RF switch VSWA2-63DR+.* [Online]. Available at https://www.minicircuits.com/WebStore/dashboard.html?model=VSWA2-63DR%2B, (cited: 27.06.2018).

[34] Murata, *Capacitor and resistor.* [Online]. Available at https://www.murata.com/en-eu/products, (cited: 27.06.2018).

[35] Keysight Techolologies, *Vector network analyzer: Hewlett Packard 8753D.* [Online]. Available at https://www.keysight.com/en/pd-1000002289%3Aepsg%3Apro-pn-8753D/network-analyzer-30-khz-to-3-ghz?cc=US&lc=eng, (cited: 27.06.2018).

[36] Rohde & Schwarz, *Microwave signal generator: Rohde & Schwarz SMP 22.* [Online]. Available at https://www.rohde-schwarz.com/fi/product/smp-productstartpage_63493-7571.html, (cited: 27.06.2018).

[37] ETS-Lindgren, *Vivaldi antenna: 3164-08 Open boundary quad-ridgen horn antenna.* [Online]. Available at http://www.ets-lindgren.com/products/antennas/open-boundary-quad-ridged-horn/4003/400304, (cited: 27.06.2018).

[38] Keysight Techolologies, *Spectrum analyzer: Agilent 8564EC.* [Online]. Available at https://www.keysight.com/en/pd-1000002099%3Aepsg%3Apro-pn-8564EC/portable-spectrum-analyzer-9-khz-to-40-ghz?cc=US&lc=eng, (cited: 27.06.2018).

[39] Keysight Techolologies, *Logic analyzer: Agilent 16902A.* [Online]. Available at https://www.keysight.com/en/pd-352524-pn-16902A/logic-analysis-system?cc=US&lc=eng, (cited: 27.06.2018).

[40] W. L. Stutzman and G. A. Thiele, *Antenna theory and design, 3rd Edition*, ch. 8 Array Antennas, pp. 271–336. Wiley, 2012.